a

Cell type		Cell line name	24h		72h	
			SAHA	NCH-51	SAHA	NCH-51
T-cell	T-ALL	Jurkat	0.90	0.72	0.63	0.75
	ATL	MT-2	>30.00	7.81	0.54	2.08
		ATL-102	>30.00	5.80	3.70	2.23
		ED-40515 (-)	1.45	0.94	0.90	0.76
B-cell	CLL	MEC2	>30.00	0.71	0.70	0.67
		MO1043	>30.00	7.67	0.76	0.79
	BL	Raji	>30.00	1.35	0.84	0.71
		Daudi	>30.00	>30.00	>30.00	11.74
	MM	U266	7.67	1.36	0.53	0.66
		XG7	>30.00	2.00	0.73	1.11
		KMS	>30.00	>30.00	1.35	3.49
		ILKM-2	1.41	1.11	0.61	0.66
		RPMI8226	5.72	1.93	2.02	2.72

Growth inhibition (%)
80-100
60-80
40-60
20-40
0-20

Each Value means IC_{50}

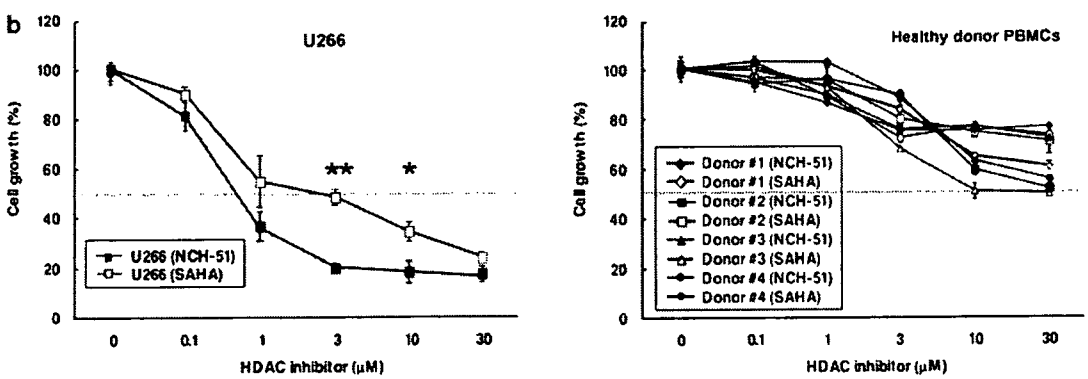

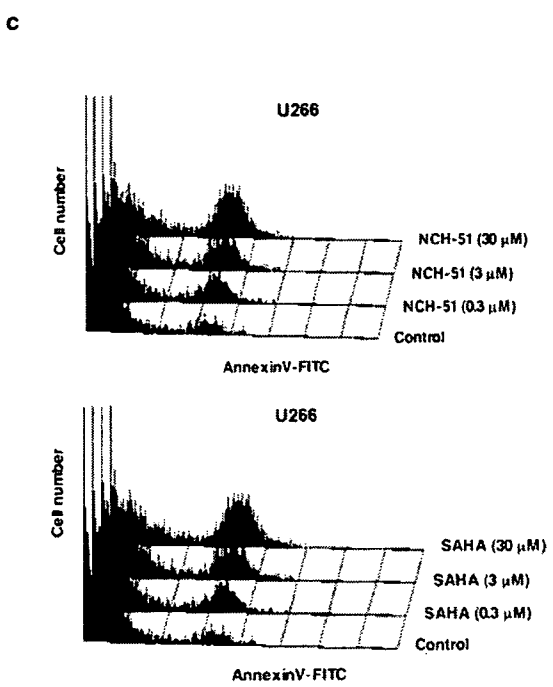

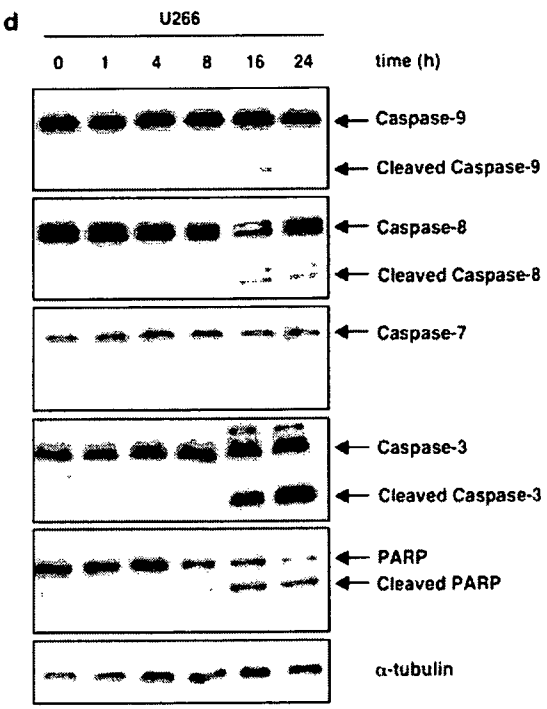

Materials and methods

Cell lines and reagents

A human acute T-cell leukemia cell line, Jurkat, ATL cell lines, MT-2, ATL-102 and ED-40515(−), chronic lymphocytic leukemia cell lines, MEC2 and MO1043, Burkitt's lymphoma cell lines, Raji and Daudi and multiple myeloma cell lines, U266, XG7, KM5, ILKM-2 and RPMI-8226 were used in this study as described previously.[20–24] For normal controls, peripheral blood mononuclear cells (PBMCs) were obtained from four independent healthy donors upon informed consent after the approval of Institutional Ethical Committee. All cells were cultured in RPMI-1640 medium, supplemented with 10% fetal bovine serum at 37°C in a 5% CO_2 incubator. NCH-51, a novel non-hydroxamate HDACi, and SAHA, a conventional hydroxamate HDACi, were synthesized by us as described previously.[11] NCH-51 and SAHA were dissolved in dimethyl sulfoxide at 50 mM and stored at −20°C. An antioxidant compound *N*-acetyl-L-cysteine (NAC) was purchased from Sigma (St Louis, MS, USA).

Growth inhibition assay

Growth inhibitory effect of HDACi was determined using 3-(4,5-dimethylthiazol-2-yl)-2,5-diphenyltetrazolium bromide assay (Sigma) as described previously.[25] Briefly, approximately $1–10 \times 10^4$ cells per 100 μl were cultured in 96-well plate in triplicates at 37°C. Optical densities (OD) at 570 and 630 nm were measured with a multiplate reader. Cell growth (%) was calculated as follows: (OD_{630}–OD_{570} of the samples/OD_{630}–OD_{570} of the control) × 100.

Apoptosis and cell cycle analysis

Apoptosis and cell cycle analyses were performed as described previously.[20] For apoptosis analysis, the cells were treated with or without HDACi for 18 h, and incubated with fluorescein isothiocyanate (FITC)-conjugated annexin V (MBL, Nagoya, Japan). The cell numbers of annexin V-positive cells were analyzed by flowcytometry (FACScan, BD Bioscience, San Jose, CA, USA) and CellQuest analysis program (BD Bioscience). For cell cycle analysis, the cells were incubated with or without HDACi for 24 h, washed with cold phosphate-buffered saline (PBS), and fixed with 70% ethanol. After incubation with RNase A (Qiagen, Alameda, CA, USA), the cell pellets were resuspended in PBS containing propidium iodide (Sigma). DNA content of each cell preparation was analyzed by flowcytometry.

Protein extraction for proteome analysis

Proteome analysis was performed according to Seike *et al.*[26] U266 cells were incubated with or without 3 μM NCH-51 for 18 h. The cell pellets were washed with cold PBS and then treated with 10%trichloroacetic acid for 30 min on ice. After washing with PBS, the pellets were collected and resuspended in lysis buffer (30 mM Tris–HCl (pH, 8.5), 7 M urea, 2 M thiourea, 3% 3-((3-chlamidopropyl) dimethylammonio)-1-propanesulfonic acid and 1% Triton X-100). Samples were then subjected to a Dounce homogenizer for 30 strokes and sonicated for 5 min in a sonicator (UCW-201, Cosmobio Co. Ltd., Tokyo, Japan). After incubation for 30 min, the samples were centrifuged at $10\,000 \times g$ for 30 min followed by ultracentrifugation at $100\,000 \times g$ for 1 h, and the supernatants were collected. Protein concentration was determined by 2D-Quant kit (GE Healthcare Bio-Sciences Corp., Piscataway, NJ, USA). Fifty micrograms of each protein extract, adjusted to pH 8.5, were labeled with 200 pmol of minimal dye CyDye (GE Healthcare Bio-Sciences Corp.). NCH-51-treated samples and untreated control proteins were labeled with Cy3 and Cy5, respectively. Internal control, consisting of half part of each paired sample was labeled with Cy2. Labeling reaction was stopped with the addition of 0.2 mM L-lysine (Sigma) for 10 min on ice. Each labeled sample was mixed into one tube and then incubated with an equal amount of lysis buffer for 10 min on ice. The final volume was adjusted to 450 μl with DeStreak Rehydration Solution and 0.5% IPG buffer (GE Healthcare Bio-Sciences Corp.).

Two-dimensional (2D) electrophoresis and image analysis

An immobilized pH gradient gel Immobiline DryStrip (GE Healthcare Bio-Sciences Corp.), with non-linear pH values (3–10), was rehydrated with the labeled protein samples at 20°C for 12 h. Isoelectric focusing was performed using IPGphor (GE Healthcare Bio-Sciences Corp.) at 20°C for total 65 000 khT. Immobiline DryStrips were then equilibrated for 15 min in the buffer (6 M urea, 1.5 M Tris–HCl (pH 8.8), 30% glycerol, 2% sodium dodecyl sulfate) containing 10 mg/ml dithiothreitol and prolonged for 15 min in the same buffer containing 25 mg/ml iodoacetamide. After equilibration, Immobiline DryStrips were transferred onto 11.5% polyacrylamide gels and run in the EttanDalt Six system (GE Healthcare Bio-Sciences Corp.) at 30 W/gel for 5 h at 20°C. The gels were scanned with appropriate wavelengths for excitation and emission using Ettan DIGE Primo (GE Healthcare Bio-Sciences Corp.). Relative quantification of spot intensities and statistical evaluation were carried out with ImageMaster 2D Platinum software (GE Healthcare Bio-Sciences Corp.). The experiments were performed in quadruplicates. The protein spots that were statisti-

Figure 1 Induction of apoptosis by a novel HDAC inhibitor NCH-51. (**a**) The growth inhibitory effects of NCH-51 and suberoylanilide hydroxamic acid (SAHA) on 13 lymphoid malignant cell lines. The cells were treated with either NCH-51 or SAHA (3 μM) for 24 or 72 h. Cell growth was estimated by 3-(4,5-dimethylthiazol-2-yl)-2,5-diphenyltetrazolium bromide (MTT) assay and gray-scale levels represent the growth inhibition rate (%) compared to untreated control. Each value indicates the mean IC_{50}. (**b**) Growth inhibitory effects of NCH-51 and SAHA on U266 cells and four control peripheral blood mononuclear cells (PBMCs). A multiple myeloma cell line U266 cells, and four healthy donor PBMCs were treated with indicated concentrations (0–30 μM) of NCH-51 (closed symbols) or SAHA (opened symbols) for 24 h. Cell growth was evaluated by MTT assay. The results are shown as the percentage cell growth compared to untreated control. These experiments were performed in triplicates and the mean values ± s.d. are shown. *$P<0.05$; **$P<0.01$. (**c**) Induction of apoptosis by NCH-51. U266 cells were treated with the indicated concentrations (0–30 μM) of NCH-51 for 18 h, stained with fluorescein isothiocyanate-conjugated annexin V, and analyzed by flowcytometry. Annexin V-positive fraction indicates the cells undergoing apoptosis. (**d**) Activation of caspases and poly-ADP ribose polymerase (PARP) cleavage by NCH-51. U266 cells were treated with 3 μM of NCH-51 for 0–24 h. Whole cell extracts were prepared and subjected to immunoblots with the indicated antibodies. Positions of uncleaved (inactivated) and cleaved (activated) caspases and PARP proteins are indicated by arrows.

cally significant between untreated control and treated sample were selected.

Protein identification by mass spectrometry

For mass spectrometric analysis, 400 μg of unlabeled-protein extract was independently applied to 2D electrophoresis. The gel was stained with DeepPurple solution (GE Healthcare Bio-Sciences Corp.) according to the manufacturer's recommendation. The gel image was obtained by scanning with Ettan DIGE Primo and matched to those of analytical gels by using the ImageMaster 2D Platinum software. The spots of interest were picked out, and in-gel protein digestion was carried out with trypsin gold (Promega, Madison, WI, USA) as described.[26] Mass spectrometric analyses were performed by using a MALDI-TOF/TOF type mass spectrometer AB4700 (Applied Biosystems, Framingham, MA, USA). The proteins were identified through the online search using MASCOT database search engine.

Immunoblot analysis

The cell extracts obtained from cell cultures treated with or without HDACi were subjected to cell extract preparation as described above. The samples were applied to electrophoresis on a 10% polyacrylamide gel and transferred onto a nitrocellulose membrane. The membranes were incubated in TBS-T (10 mM Tris–HCl (pH, 8.0), 150 mM NaCl, 0.1% Tween) with 5% non-fat milk containing 1:1000 diluted primary antibodies against either caspase-9, -8, -7, -3, poly-ADP ribose polymerase (PARP) (Cell Signaling Technology, Danvers, MA, USA), peroxiredoxin 1 (Affinity Bioreagents, Golden, CO, USA), elongation factor-2 or α-tubulin (Santa Cruz, Santa Cruz, CA, USA). Membranes were then rinsed in TBS-T and further incubated with HRP-conjugated secondary antibody (GE Healthcare Bio-Sciences Corp.) in TBS-T with 5% non-fat milk. Each protein was detected by SuperSignal (PIERCE, Rockford, IL, USA).

Detection of ROS

ROS content was measured as described previously.[27] After treatment with HDACi, the cells were incubated with an oxidation-sensitive fluorescent probe 2′, 7′-dichlorofluorescein diacetate (H_2-DCFDA) (Molecular Probes Inc., Eugene, OR, USA) at a final concentration of 5 μM for 30 min. The cells were washed and resuspended in PBS, and then ROS amount was measured by flowcytometry.

Results

NCH-51 induces apoptosis greater than SAHA

We first evaluated the growth inhibitory effects of NCH-51 on a variety of lymphoid malignant cell lines (Figure 1a). A tentative result in a multiple myeloma cell line U266 cells is shown in Figure 1b. In most of the cell lines including U266 cells, NCH-51 exhibited a stronger growth inhibitory effect than SAHA at 3 μM for 24 h treatment, whereas prolonged incubation for 72 h did not show such a difference. It is noted that there was no significance in the growth inhibitory effect on four healthy donor PBMCs between NCH-51 and SAHA (IC_{50} values of both agents were higher than 30 μM), suggesting a cell-type specific cytotoxicity of NCH-51. We then analyzed the apoptosis and cell cycle distribution after the treatment with NCH-51 or SAHA. In the six cell lines (Jurkat, ED-40515(−), MEC2, U266, XG7 and ILKM-2), all of which showed a high susceptibility to NCH-51 ($IC_{50}<3$ μM), NCH-51 strongly induced apoptosis greater than SAHA after 24 h treatment as demonstrated by generation of sub-G_1 cells (Figure 1c and Table 1). In fact, when U266 cells were treated with NCH-51, cleaved forms of caspase-9, -8, -3 and PARP could be detected after 8 h, evidently at 16 h, although no activation of caspase-7 was detected (Figure 1d), suggesting that NCH-51 induces apoptosis through both extrinsic (type I) and intrinsic (type II) pathways[28] in the short-term treatment. On the other hand, cell cycle analysis revealed that NCH-51 increased the cell number at G_2/M-phase and reduced the number at G_1- or S-phase in most of the cell lines examined (Table 1, right column). No significant difference in the effects on cell cycle regulation was observed between NCH-51- and SAHA-treated cells. These observations suggest that the apoptosis-inducing activity might be attributable to the difference in the observed growth inhibitory effects between NCH-51 and SAHA.

NCH-51 regulates the expressions of antioxidant molecules at the protein level

To identify the target molecules regulated by NCH-51, we analyzed the RNA and protein expression profiles. cDNA microarray analysis using U266 cells showed that NCH-51 treatment upregulated the expression of *p21* and *p19* (Supplementary Table 1), confirming the previous reports by us[11] and others.[12–14] On the other hand, NCH-51 downregulated the gene expression of *CFLAR* (*c-FLIP*), *survivin* and *BCL2L2 (bcl-w)*, which act as antiapoptotic molecules. These results suggested that these genes were responsible for the growth inhibitory action of NCH-51, however, there was no notable difference in mRNA expression between NCH-51- and SAHA-treated cells. We then performed the proteome analysis. Whole cell extracts were prepared from U266 cells treated with or without NCH-51, and the protein samples were labeled with fluorescent dyes and applied to 2D electrophoresis (Figure 2a). By comparing the amounts of cellular proteins, we identified 14 proteins that varied relatively to NCH-51 treatment (Table 2). Ten proteins including nucleotide diphosphate kinase A (NDPKA), peroxiredoxin 1 and 2 (PRDX1, 2), glutathione *S*-transferase P1-1 (GSTP1-1), 14-3-3 zeta/delta, Cl^- intracellular channel proteins 1 and 4 (CLIC1, 4), proteasome subunit α3, protease activator 28 β subunit and Rho GDI α were upregulated, and four proteins including alanyl-tRNA synthetase (AARS), elongation factor-2 (EF-2), heat-shock 70 kDa protein 8 (HSPA8) and mitochondrial inner membrane protein, were downregulated after the treatment with NCH-51. Interestingly, some of these proteins upregulated by NCH-51 belong to a class of antioxidant molecules. It is noted that PRDX1 and PRDX2 were upregulated at both mRNA and protein levels, thus they are considered to be upregulated at the gene expression level, whereas most of the proteins were upregulated without induction at the gene expression level. In contrast, EF-2 and HSPA8 were downregulated at the protein level. The effects of NCH-51 and SAHA on the expression of EF-2 and PRDX1 were then verified. As shown in Figure 2b, EF-2 protein level was decreased either by NCH-51 or SAHA in the cell lines such as U266, ED-40515 (−) and XG7 cells that were highly susceptible to HDACi. EF-2 was decreased after 16 h treatment with these HDACi (data not shown). On the other hand, in the cell lines such as MEC2, Daudi and KM5 cells that were less sensitive to HDACi, EF-2 protein level was not significantly changed. PRDX1 protein level was upregulated by the treatment with either NCH-51 or SAHA in ED-40515 (−), U266, XG7 and MEC2 cells. SAHA seemed to upregulate PRDX1 more than NCH-51.

Table 1 The profiles of apoptosis and cell cycle distribution

Cell line	*HDAC inhibitor (μM)*	*Apoptotic cell[a] (%)*	*Cell cycle distribution[a](%)*			
			sub G_1	*G_1*	*S*	*G_2/M*
Jurkat	Untreated control	6.30	5.11	50.39	20.76	20.64
	SAHA					
	3 μM	13.45	28.56	9.15	12.97	46.22
	30 μM	28.97	32.39	7.06	18.10	40.83
	NCH-51					
	3 μM	19.27	42.66	8.05	10.04	36.28
	30 μM	35.45	42.69	7.64	14.41	32.21
MT-2	Untreated control	6.84	3.02	63.25	15.29	15.64
	SAHA					
	3 μM	8.23	9.41	49.04	11.70	26.36
	30 μM	8.75	10.35	62.95	6.15	13.96
	NCH-51					
	3 μM	8.45	3.26	62.21	16.34	16.53
	30 μM	8.62	5.38	71.64	8.35	12.22
ED-40515 (–)	Untreated control	6.44	8.40	46.82	23.30	19.67
	SAHA					
	3 μM	20.74	18.88	21.41	19.07	36.90
	30 μM	20.12	26.87	22.20	20.49	27.75
	NCH-51					
	3 μM	22.12	27.10	28.04	19.04	23.91
	30 μM	21.33	26.54	25.09	20.56	25.72
MEC2	Untreated control	3.20	5.66	60.06	19.96	12.16
	SAHA					
	3 μM	4.84	12.32	37.33	19.84	26.70
	30 μM	8.22	18.14	29.46	22.63	25.12
	NCH-51					
	3 μM	6.50	16.22	36.43	19.28	24.75
	30 μM	11.08	21.24	30.47	20.93	23.29
MO1043	Untreated control	4.14	0.89	54.88	20.75	17.87
	SAHA					
	3 μM	4.30	3.45	68.83	7.49	15.41
	30 μM	15.96	18.85	48.29	6.62	23.14
	NCH-51					
	3 μM	3.74	2.47	73.90	7.17	12.88
	30 μM	14.93	21.75	48.79	6.14	21.03
Daudi	Untreated control	1.62	1.62	52.02	22.77	19.55
	SAHA					
	3 μM	2.08	2.17	23.65	22.33	46.30
	30 μM	2.12	2.34	22.83	19.75	48.21
	NCH-51					
	3 μM	2.64	1.90	50.38	14.74	27.71
	30 μM	3.04	2.19	25.68	22.19	43.28
U266	Untreated control	6.17	6.30	67.42	10.99	13.02
	SAHA					
	3 μM	17.65	11.91	56.24	10.35	19.72
	30 μM	29.73	17.06	48.70	12.69	19.68
	NCH-51					
	3 μM	22.90	13.39	54.07	11.60	18.62
	30 μM	32.63	18.90	49.15	13.40	18.94
XG7	Untreated control	7.27	7.58	49.21	20.34	23.37
	SAHA					
	3 μM	8.74	8.50	50.40	8.33	28.32
	30 μM	9.43	15.38	34.23	15.10	28.21
	NCH-51					
	3 μM	11.47	10.00	49.32	8.62	28.62
	30 μM	13.13	17.87	35.44	14.67	27.93
KM5	Untreated control	4.24	2.91	42.15	27.85	23.43
	SAHA					
	3 μM	4.30	6.32	31.85	31.44	26.13
	30 μM	15.96	23.37	20.62	26.19	24.68
	NCH-51					
	3 μM	3.74	6.75	38.34	29.96	20.84
	30 μM	18.46	20.33	27.77	23.29	24.31

Table 1 (*Continued*)

Cell line	HDAC inhibitor (μM)	Apoptotic cell[a] (%)	Cell cycle distribution[a](%)			
			sub G_1	G_1	S	G_2/M
ILKM-2	Untreated control	7.35	4.07	58.61	13.05	22.89
	SAHA					
	3 μM	7.84	8.97	61.53	6.23	22.12
	30 μM	21.41	20.63	51.10	12.71	13.88
	NCH-51					
	3 μM	8.71	6.04	63.21	6.93	22.45
	30 μM	30.04	20.54	51.45	12.15	15.13

Abbreviations: HDAC, histone deacetylase; SAHA, suberoylanilide hydroxamic acid.
[a]Each value shows the average of 20000 cells counted.

NCH-51 induces cytotoxic effect through the modulation of intracellular ROS

From the results of proteome analyses, NCH-51 appeared to promote the expression of antioxidant molecules, either at the transcriptional or post-transcriptional level, which prompted us to examine the effect of NCH-51 on the levels of ROS accumulation. Interestingly, the temporal profile of ROS amount in U266 cells treated with NCH-51 appeared to be in a concave shape indicating a gradual suppression of ROS accumulation within the initial 4 h and subsequent induction of ROS (Figure 3a), whereas the temporal profile with SAHA continuously declined over time. Similar trends were observed with other cell lines (data not shown). As summarized in Table 2, SAHA was more effective in reducing ROS than NCH-51, and the difference in ROS amount between NCH-51 and SAHA was most evident at 24 h, when the difference in growth inhibitory effect could be observed (Figure 1). These results suggested a possibility that dynamic state of ROS in each cell could be attributed to the growth inhibitory effect of HDACi. We thus examined whether NAC, a small-molecule antioxidant compound, could modulate the effect of NCH-51 (Figure 3b). Expectedly, when U266 cells were pretreated with NAC, the NCH-51-mediated cell growth inhibition was abolished. Similar effect was observed in SAHA-treated cells as much as in NCH-51-treated cells (data not shown). These results indicated that high amount of ROS might be necessary for the induction of NCH-51-mediated cytotoxicity.

Discussion

There have been accumulating reports of successful inhibition of cancer cell growth using small-molecule HDACi compounds.[1,7] Initial studies with SAHA indicated that the mode of action of HDACi might be through upregulating the transcriptionally repressed genes during carcinogenic processes by acetylating the repressive histones.[12–14] However, recent reports have demonstrated that HDACi compounds also exert anticancer effects through acetylation of non-histone substrates.[15–19] For example, HDAC6, a microtubule-associated deacetylase, was shown to be responsible for transportation of misfolded proteins to aggresome thus promoting protein degradation.[19,29] Thus, we have attempted to clarify the mechanism of anticancer effects of NCH-51 by examining both mRNA and protein levels.

In this study, we noticed that NCH-51 induced apoptosis in sensitive cell lines greater than SAHA (Figures 1 and 2a and Table 1). Analyses of mRNA expression levels in NCH-51- and SAHA-treated cells has revealed that transcriptional repression of antiapoptotic genes, such as *survivin*, *bcl-w* and *c-FLIP* and upregulation of cell cycle regulators, such as *p21* and *p19*, could be attributable to the induction of apoptosis and cell cycle arrest, respectively (Supplementary Table 1, 2 and Supplementary Figure 1), supporting the previous findings by others.[12–14] There was no difference in the mRNA expression level between NCH-51- and SAHA-treated samples (Supplementary Figure 1). We have confirmed no difference in inducing activity for acetylation of histone H4 between these two HDACi's (Supplementary Figure 2). These findings suggest that NCH-51 and SAHA similarly affect gene expression presumably through histone acetylation. We thus examined the effects of these compounds on protein expression profile to understand the difference between NCH-51 and SAHA at the post-transcriptional level.

Interestingly, our proteome analyses revealed the upregulation of some antioxidant molecules including PRDX1, PRDX2 and GSTP1-1 (Table 2 and Figure 2). In addition, previous reports indicated that some other proteins identified by the present proteome analysis (Table 2) could be activated by oxidative stress.[30–34] For example, NDPKA is reported to be activated by ROS and protected the cell from ROS-induced apoptosis.[30,31] CLIC1 protein contains a redox-active site and is activated during ROS-triggered apoptosis.[32,33] These findings suggested a possibility that NCH-51 might induce the cytotoxic effect by modulating the intracellular ROS content. In fact, pretreatment with NAC abolished the growth inhibitory effect of NCH-51 (Figure 3b). These results support the previous findings by others, which showed the ROS accumulation by HDACi.[14,34,35] However, in contrast to the previous reports, both NCH-51 and SAHA downregulated the ROS content after 24 h treatment in most of the cell lines tested except for KM5 cells, in which ROS was increased by the treatment with SAHA or NCH-51 (Table 3). These findings were reproducibly observed. Although we currently do not know the reason why there was a discrepancy between our study and others, we think the time-point and/or cell characteristics may be different between them. When temporal profiles of ROS accumulation were examined (Figure 3a), we found a typical bimodal kinetics of the intracellular ROS content after treatment with NCH-51; an initial downregulation and subsequent upregulation of ROS. On the other hand, SAHA did not follow the similar kinetics and the intracellular ROS level gradually and continuously decreased (Figure 3a). Therefore, it is possible that apparent differences in the ability of cell growth inhibition between NCH-51 and SAHA, may be explained through the different effects on the redox status of cells and induction of antioxidant proteins. Interestingly, our proteome/transcriptome analyses have revealed that the upregulation of antioxidant molecules occurred at either protein or mRNA levels: GSTP1-1 was upregulated by

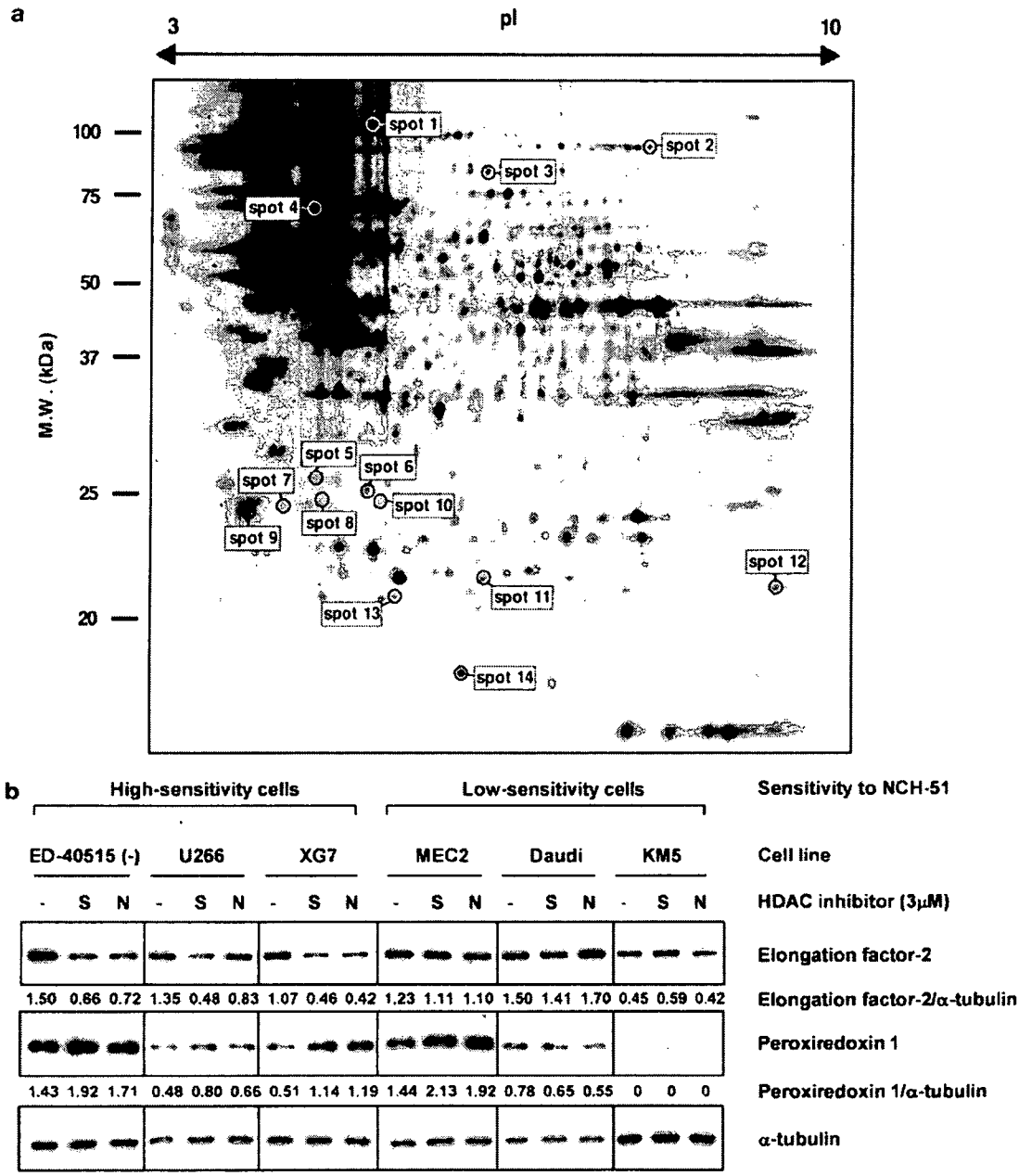

Figure 2 Proteome analysis of the effects of NCH-51. (**a**). 2D electrophoresis image of whole cell proteins prepared from U266 cells. After U266 cells were treated with or without 3 μM NCH-51 for 18 h, the whole cell extracts were prepared and applied to 2D electrophoresis in quadruplicates. Fourteen spots, whose relative amounts were either increased or decreased by the treatment with NCH-51 in all four gels, were indicated. Each spot number in the image corresponds to those in Table 2. MW, molecular weight (kDa). pI, isoelectric point. (**b**) Downregulation of elongation factor-2 (EF-2) and upregulation of peroxiredoxin 1 (PRDX1) by HDACi. The cells were treated with suberoylanilide hydroxamic acid (S) or NCH-51 (N) (3 μM) for 18 h. Whole cell extracts were prepared and subjected to immunoblots with the indicated antibodies. Each value means the ratio of the protein amount to α-tubulin (internal control).

NCH-51 only at the protein level, and PRDX1 and PRDX2 were upregulated primarily at the transcriptional level. These findings suggest that there may be two consequent antioxidative mechanisms by which HDACi modulate ROS accumulation: (i) the mRNA level, acting through induction of transcription of antioxidant molecules *de novo*, and (ii) the protein level, which was presumably caused by blocking the cellular protein transport/degradation pathway involving aggresome and proteasome. Importantly, we have observed that SAHA but not NCH-51 could induce acetylations of α-tubulin and HSP90 (Supplementary Figure 2), suggesting that SAHA might prolong the latter mechanism through blocking the degradation of antioxidant molecules. In fact, SAHA seemed to increase protein expression of PRDX1 greater than NCH-51 (Figure 2b). Since NCH-51 does not retain antioxidant molecules at the protein level, it induces the accumulation of ROS. Cellular levels of antioxidant molecules have been reported to be associated with the sensitivity to conventional anticancer agents.[36] Therefore,

Table 2 Upregulated/downregulated proteins after the treatment with NCH-51 in U266 cells

Spot no.	*Protein ID*	*Protein name*	*MW*	*pI*	*Protein ratio (T/C)*[a]	*mRNA ratio (T/C)*[a]
1	NP_001596	Alanyl-tRNA synthetase (AARS)	106734	5.31	0.80	0.74
2	NP_001952	Elongation factor-2 (EF-2)	95146	6.42	0.82	1.23
3	NP_006830	Mitochondrial inner membrane protein (IMMT)	83626	6.08	0.83	0.64
4	NP_006588	Heat-shock 70 kDa protein 8 (HSPA8)	70854	5.28	0.82	1.18
5	NP_001279	Cl^- intracellular channel protein 1 (CLIC1)	26775	5.09	1.34	0.67
6	NP_002809	Protease activator 28 β subunit (PA28β)	27213	5.44	1.54	1.03
7	NP_004300	Rho GDP-dissociation inhibitor 1 (Rho GDIα)	23193	5.02	1.42	0.92
8	NP_002779	Proteasome subunit α type3	28284	5.19	1.32	0.73
9	NP_663723	14-3-3 ζ/δ (PKC inhibitor protein 1)	28828	4.73	1.37	0.83
10	NP_039234	Cl intracellular channel protein 4 (CLIC4)	28754	5.45	1.38	0.86
11	NP_000843	Glutathione S-transferase P 1–1(GSTP1-1)	23210	5.44	1.38	0.98
12	NP_002565	Peroxiredoxin 1 (thioredoxin peroxidase 2) (PRDX1)	22096	8.27	1.30	1.4
13	NP_005800	Peroxiredoxin 2 (thioredoxin peroxidase 1) (PRDX2)	21747	5.67	1.30	1.35
14	NP_000260	Nucleoside disphosphate kinase A (NDPKA)	17138	5.83	1.50	1.04

[a]The results are indicated as the ratio of NCH-51-treated sample to untreated control (T/C).

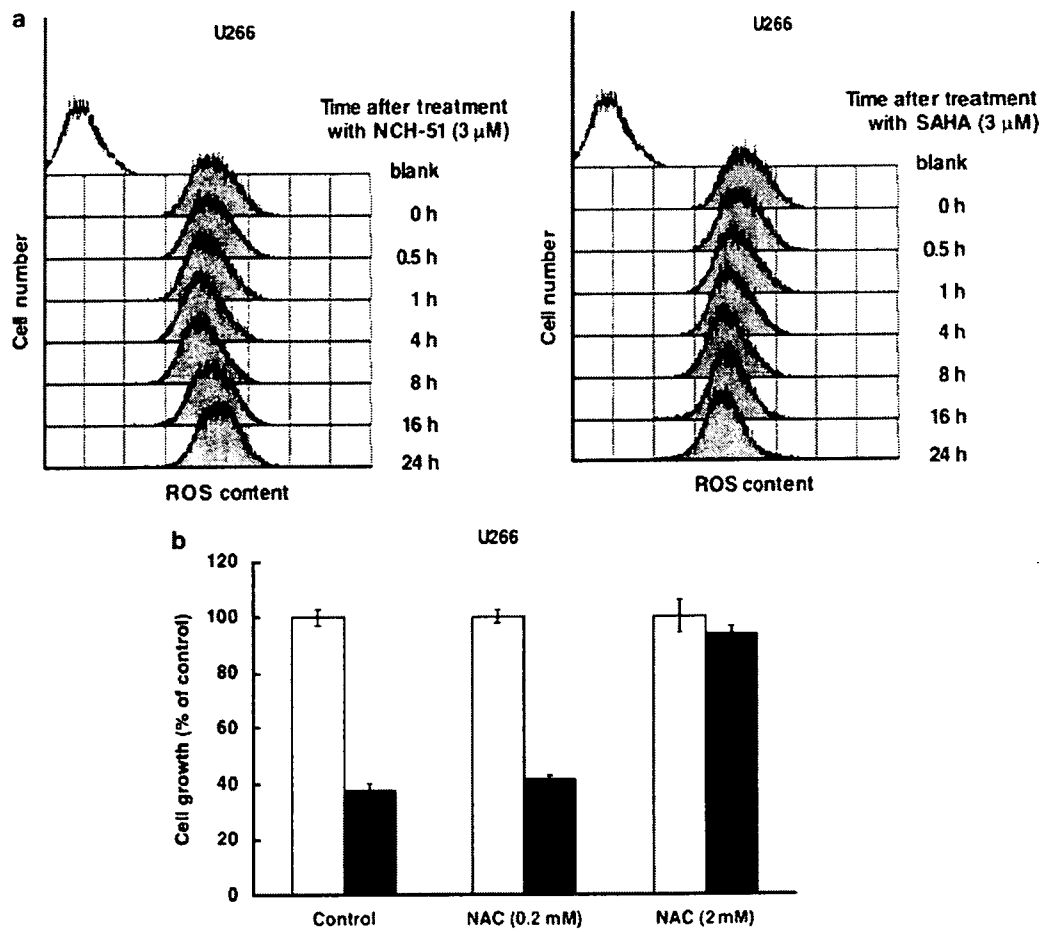

Figure 3 Effects of NCH-51 and suberoylanilide hydroxamic acid (SAHA) on reactive oxygen species (ROS) accumulation. (**a**) Time course of intracellular ROS after the treatment with HDACi. U266 cells were treated with NCH-51 or SAHA (3 μM) given the indicated time (0–24 h). After the treatment, H_2-DCFDA was added and further incubated for 30 min. ROS content was measured by flowcytometry. Blank, H_2-DCFDA-untreated control. (**b**) Effects of *N*-acetyl-L-cysteine (NAC) on the NCH-51-induced cell growth inhibition. U266 cells were treated with or without NCH-51 (3 μM) for 24 h in the presence or absence of NAC (0.2 or 2 mM). Cell growth was measured by 3-(4,5-dimethylthiazol-2-yl)-2,5-diphenyltetrazolium bromide assay. Open and closed bars indicate untreated and the NCH-51-treated cells. The results are shown as the percentage compared to untreated control. Experiments were done in triplicates and the mean values $\pm$ s.d. are shown.

NCH-51 can not only induce apoptosis through ROS accumulation, but also enhance the cytotoxicity of other agents in the combination treatment more efficiently than SAHA.

Our proteome analysis has also identified several proteins other than antioxidant molecules, including EF-2, AARS and HSPA8. We confirmed that EF-2 protein, a member of the GTP-

Table 3 ROS content and growth inhibitory effect after the treatment with HDAC inhibitor

Cell line	*ROS content (% of control)*[a]		*Growth inhibition (% of control)*[b]	
	NCH-51 (3 μM)	*SAHA (3 μM)*	*NCH-51 (3 μM)*	*SAHA (3 μM)*
Jurkat	86	47	63.5±0.8	37.7±2.5
MT-2	100	100	38.8±0.3	11.0±2.3
ED-40515 (−)	82	56	71.2±1.2	44.1±1.0
MEC2	59	46	41.3±1.1	3.5±2.8
MO1043	91	65	46.0±0.5	7.2±2.9
Daudi	74	54	25.6±1.8	15.1±3.0
U266	95	85	80.7±1.8	51.7±3.2
XG7	74	28	66.5±1.1	23.1±1.6
KM5	126	119	20.5±0.5	14.6±1.2
ILKM-2	94	94	85.5±0.2	81.3±1.1

Abbreviations: HDAC, histone deacetylase; ROS, reactive oxygen species; SAHA, suberoylanilide hydroxamic acid.
[a]Each value shows the average of 20 000 cells counted.
[b]Each value shows the mean±s.d.

binding translational elongation factor family,[37] was specifically decreased in high-sensitivity cell lines such as ED-40515 (−) and U266 cells (Figure 2b) after 16 h treatment (data not shown). However, gene expression of EF-2 was upregulated after the treatment with NCH-51 (Table 2). This discrepancy indicates a possibility that NCH-51 could induce rapid turnover of EF-2 protein followed by upregulation of RNA expression. Similar effects on EF-2 were also observed with SAHA (Figure 2b). Since EF-2 has been reported to be inactivated by ROS and lead to inhibition of translation,[38] it is suggested that locally induced ROS by HDACi might induce EF-2 inactivation and degradation presumably by direct oxidation. Although the mechanism by which EF-2 is downregulated by HDACi remains unclear, EF-2 may be used as a feasible surrogate marker to evaluate the susceptibility of HDACi. Similar to EF-2, AARS and HSPA8 were downregulated at the protein level. It is known that HSPA8 are involved in protein folding and transport.[39] Thus, these findings collectively suggest that NCH-51 might arrest protein synthesis and transportation.

In conclusion, our study demonstrates the therapeutic advantage of NCH-51 on growth inhibition of lymphoid malignant cells. Importantly, NCH-51 did not affect the cell growth of normal PBMCs with the effective concentrations on malignant cells (Figure 1b). In addition to its therapeutic efficacy and selectivity, NCH-51 has additional advantages in clinical use based on its pharmacological features. Therefore, NCH-51 could be a useful anticancer agent against lymphoid malignancies.

Acknowledgements

We thank Mr ME Cueno for language editing. This work is supported in part by grant-in-aids from the Ministry of Education, Culture, Sports, Science and Technology and the Ministry of Health, Labor and Welfare of Japan. TS is supported by a grant of Aichi Cancer Research Foundation and a grant of Oujinkai Foundation. HN, TS and NY are supported by a grant of Takeda Science Foundation.

References

1 Minucci S, Pelicci PG. Histone deacetylase inhibitors and the promise of epigenetic (and more) treatments for cancer. *Nat Rev Cancer* 2006; **6**: 38–51.
2 Strahl BD, Allis CD. The language of covalent histone modifications. *Nature* 2000; **403**: 41–45.
3 Turner BM. Cellular memory and the histone code. *Cell* 2002; **111**: 285–291.
4 Claus R, Lubbert M. Epigenetic targets in hematopoietic malignancies. *Oncogene* 2003; **22**: 6489–6496.
5 Fraga MF, Ballestar E, Villar-Garea A, Boix-Chornet M, Espada J, Schotta G *et al*. Loss of acetylation at Lys16 and trimethylation at Lys20 of histone H4 is a common hallmark of human cancer. *Nat Genet* 2005; **37**: 391–400.
6 Seligson DB, Horvath S, Shi T, Yu H, Tze S, Grunstein M *et al*. Global histone modification patterns predict risk of prostate cancer recurrence. *Nature* 2005; **435**: 1262–1266.
7 Kelly WK, Marks PA. Drug insight: histone deacetylase inhibitors–development of the new targeted anticancer agent suberoylanilide hydroxamic acid. *Nat Clin Pract Oncol* 2005; **2**: 150–157.
8 Kelly WK, O'Connor OA, Krug LM, Chiao JH, Heaney M, Curley T *et al*. Phase I study of an oral histone deacetylase inhibitor, suberoylanilide hydroxamic acid, in patients with advanced cancer. *J Clin Oncol* 2005; **23**: 3923–3931.
9 Ryan QC, Headlee D, Acharya M, Sparreboom A, Trepel JB, Ye J *et al*. Phase I and pharmacokinetic study of MS-275, a histone deacetylase inhibitor, in patients with advanced and refractory solid tumors or lymphoma. *J Clin Oncol* 2005; **23**: 3912–3922.
10 Golub LM, Lee HM, Ryan ME, Giannobile WV, Payne J, Sorsa T. Tetracyclines inhibit connective tissue breakdown by multiple non-antimicrobial mechanisms. *Adv Dent Res* 1998; **12**: 12–26.
11 Suzuki T, Nagano Y, Kouketsu A, Matsuura A, Maruyama S, Kurotaki M *et al*. Novel inhibitors of human histone deacetylases: design, synthesis, enzyme inhibition, and cancer cell growth inhibition of SAHA-based non-hydroxamates. *J Med Chem* 2005; **48**: 1019–1032.
12 Huang L, Sowa Y, Sakai T, Pardee AB. Activation of the p21WAF1/CIP1 promoter independent of p53 by the histone deacetylase inhibitor suberoylanilide hydroxamic acid (SAHA) through the Sp1 sites. *Oncogene* 2000; **19**: 5712–5719.
13 Richon VM, Sandhoff TW, Rifkind RA, Marks PA. Histone deacetylase inhibitor selectively induces p21WAF1 expression and gene-associated histone acetylation. *Proc Natl Acad Sci USA* 2000; **97**: 10014–10019.
14 Rosato RR, Almenara JA, Grant S. The histone deacetylase inhibitor MS-275 promotes differentiation or apoptosis in human leukemia cells through a process regulated by generation of reactive oxygen species and induction of p21CIP1/WAF1 1. *Cancer Res* 2003; **63**: 3637–3645.
15 Bali P, Pranpat M, Bradner J, Balasis M, Fiskus W, Guo F *et al*. Inhibition of histone deacetylase 6 acetylates and disrupts the chaperone function of heat shock protein 90: a novel basis for antileukemia activity of histone deacetylase inhibitors. *J Biol Chem* 2005; **280**: 26729–26734.
16 Hubbert C, Guardiola A, Shao R, Kawaguchi Y, Ito A, Nixon A *et al*. HDAC6 is a microtubule-associated deacetylase. *Nature* 2002; **417**: 455–458.

17 Insinga A, Monestiroli S, Ronzoni S, Carbone R, Pearson M, Pruneri G *et al.* Impairment of p53 acetylation, stability and function by an oncogenic transcription factor. *EMBO J* 2004; **23**: 1144–1154.
18 Chen L, Fischle W, Verdin E, Greene WC. Duration of nuclear NF-kappaB action regulated by reversible acetylation. *Science* 2001; **293**: 1653–1657.
19 Hideshima T, Bradner JE, Wong J, Chauhan D, Richardson P, Schreiber SL *et al.* Small-molecule inhibition of proteasome and aggresome function induces synergistic antitumor activity in multiple myeloma. *Proc Natl Acad Sci USA* 2005; **102**: 8567–8572.
20 Sanda T, Asamitsu K, Ogura H, Iida S, Utsunomiya A, Ueda R *et al.* Induction of cell death in adult T-cell leukemia cells by a novel IkappaB kinase inhibitor. *Leukemia* 2006; **20**: 590–598.
21 Uranishi M, Iida S, Sanda T, Ishida T, Tajima E, Ito M *et al.* Multiple myeloma oncogene 1 (MUM1)/interferon regulatory factor 4 (IRF4) upregulates monokine induced by interferon-gamma (MIG) gene expression in B-cell malignancy. *Leukemia* 2005; **19**: 1471–1478.
22 Pulvertaft JV. Cytology of Burkitt's tumour (African lymphoma). *Lancet* 1964; **39**: 238–240.
23 Klein E, Klein G, Nadkarni JS, Nadkarni JJ, Wigzell H, Clifford P. Surface IgM-kappa specificity on a Burkitt lymphoma cell *in vivo* and in derived culture lines. *Cancer Res* 1968; **28**: 1300–1310.
24 Suzuki A, Iida S, Kato-Uranishi M, Tajima E, Zhan F, Hanamura I *et al.* ARK5 is transcriptionally regulated by the Large-MAF family and mediates IGF-1-induced cell invasion in multiple myeloma: ARK5 as a new molecular determinant of malignant multiple myeloma. *Oncogene* 2005; **24**: 6936–6944.
25 Sanda T, Iida S, Ogura H, Asamitsu K, Murata T, Bacon KB *et al.* Growth inhibition of multiple myeloma cells by a novel IkappaB kinase inhibitor. *Clin Cancer Res* 2005; **11**: 1974–1982.
26 Seike M, Kondo T, Mori Y, Gemma A, Kudoh S, Sakamoto M *et al.* Proteomic analysis of intestinal epithelial cells expressing stabilized beta-catenin. *Cancer Res* 2003; **63**: 4641–4647.
27 Imai K, Nakata K, Kawai K, Hamano T, Mei N, Kasai H *et al.* Induction of OGG1 gene expression by HIV-1 Tat. *J Biol Chem* 2005; **280**: 26701–26713.
28 Opferman JT, Korsmeyer SJ. Apoptosis in the development and maintenance of the immune system. *Nat Immunol* 2003; **4**: 410–415.
29 Kawaguchi Y, Kovacs JJ, McLaurin A, Vance JM, Ito A, Yao TP. The deacetylase HDAC6 regulates aggresome formation and cell viability in response to misfolded protein stress. *Cell* 2003; **115**: 727–738.
30 Song EJ, Kim YS, Chung JY, Kim E, Chae SK, Lee KJ. Oxidative modification of nucleoside diphosphate kinase and its identification by matrix-assisted laser desorption/ionization time-of-flight mass spectrometry. *Biochemistry* 2000; **39**: 10090–10097.
31 Arnaud-Dabernat S, Masse K, Smani M, Peuchant E, Landry M, Bourbon PM *et al.* Nm23-M2/NDP kinase B induces endogenous c-myc and nm23-M1/NDP kinase A overexpression in BAF3 cells. Both NDP kinases protect the cells from oxidative stress-induced death. *Exp Cell Res* 2004; **301**: 293–304.
32 Harrop SJ, DeMaere MZ, Fairlie WD, Reztsova T, Valenzuela SM, Mazzanti M *et al.* Crystal structure of a soluble form of the intracellular chloride ion channel CLIC1 (NCC27) at 1.4-A resolution. *J Biol Chem* 2001; **276**: 44993–45000.
33 Shimizu T, Numata T, Okada Y. A role of reactive oxygen species in apoptotic activation of volume-sensitive Cl(−) channel. *Proc Natl Acad Sci USA* 2004; **101**: 6770–6773.
34 Ruefli AA, Ausserlechner MJ, Bernhard D, Sutton VR, Tainton KM, Kofler R *et al.* The histone deacetylase inhibitor and chemotherapeutic agent suberoylanilide hydroxamic acid (SAHA) induces a cell-death pathway characterized by cleavage of Bid and production of reactive oxygen species. *Proc Natl Acad Sci USA* 2001; **98**: 10833–10838.
35 Ungerstedt JS, Sowa Y, Xu WS, Shao Y, Dokmanovic M, Perez G *et al.* Role of thioredoxin in the response of normal and transformed cells to histone deacetylase inhibitors. *Proc Natl Acad Sci USA* 2005; **102**: 673–678.
36 Yokomizo A, Ono M, Nanri H, Makino Y, Ohga T, Wada M *et al.* Cellular levels of thioredoxin associated with drug sensitivity to cisplatin, mitomycin C, doxorubicin, and etoposide. *Cancer Res* 1995; **55**: 4293–4296.
37 Ryazanov AG, Shestakova EA, Natapov PG. Phosphorylation of elongation factor 2 by EF-2 kinase affects rate of translation. *Nature* 1988; **334**: 170–173.
38 Patel J, McLeod LE, Vries RG, Flynn A, Wang X, Proud CG. Cellular stresses profoundly inhibit protein synthesis and modulate the states of phosphorylation of multiple translation factors. *Eur J Biochem* 2002; **269**: 3076–3085.
39 Young JC, Agashe VR, Siegers K, Hartl FU. Pathways of chaperone-mediated protein folding in the cytosol. *Nat Rev Mol Cell Biol* 2004; **5**: 781–791.

Supplementary Information accompanies the paper on the Leukemia website (http://www.nature.com/leu)

RAPID COMMUNICATIONS IN MASS SPECTROMETRY
Rapid Commun. Mass Spectrom. 2007; 21: 3815–3824
Published online in Wiley InterScience (www.interscience.wiley.com) DOI: 10.1002/rcm.3279

RCM

Efficient identification and quantification of proteins using isotope-coded 1-(6-methylnicotinoyloxy)-succinimides by matrix-assisted laser desorption/ionization time-of-flight mass spectrometry

Hiroki Tsumoto[1,3], Chie Murata[2], Naoki Miyata[3], Kohfuku Kohda[1]* and Ryo Taguchi[2]

[1]Research Institute of Pharmaceutical Sciences, Musashino University, Shinmachi Nishitokyo-shi, Tokyo 202-8585, Japan
[2]Department of Metabolome, Graduate School of Medicine, The University of Tokyo, Hongo, Bunkyo-ku, Tokyo 113-0033, Japan
[3]Graduate School of Pharmaceutical Sciences, Nagoya City University, Tanabe-dori, Mizuho-ku, Nagoya 467-8603, Japan

Received 6 March 2007; Revised 26 August 2007; Accepted 30 September 2007

We describe a convenient and useful method for the identification and relative quantification of proteins using light and heavy reagents, 1-(6-methylnicotinoyloxy)succinimides (6-CH_3-Nic-NHS and 6-CD_3-Nic-NHS, respectively). This method is based on the chemical derivatization of amino groups of tryptic peptides with these reagents, i.e., the basic moiety of the reagents thus incorporated into both the N-terminal amino group and the ε-amino group of the lysine residue would improve the ionization efficiency of tryptic peptides. An increase in protein sequence coverage is achieved by derivatization with these reagents or by combination of mass values before and after derivatization. Since a combination of 6-CH_3-Nic-NHS and d_3-labeled reagent (6-CD_3-Nic-NHS) generates a 3 Da mass difference per reaction site, the d_3-labeled reagent shifts the mass values of d_0-labeled peptides according to the number of reactive amino groups in the peptides. In the case of tryptic peptides, the mass values of C-terminal arginine and lysine peptides are shifted by 3 and 6 Da, respectively. Further, the 3 Da mass difference between 6-CH_3-Nic-NHS and 6-CD_3-Nic-NHS offers a means for the relative quantification of protein by matrix-assisted laser desorption/ionization time-of-flight mass spectrometry.

Mass spectrometry (MS) has been successfully used for the identification of proteins. Peptide mass fingerprinting (PMF) by matrix-assisted laser desorption/ionization time-of-flight MS (MALDI-TOF MS) is one of the most widely used methods for protein identification. The mass values of tryptic peptides derived from protein digestion are matched to those of theoretical peptides by database search such as MASCOT. To identify the parent protein with high accuracy and confidence, the number of matched tryptic peptides is important. Park *et al.* have reported the dansylation of tryptic peptides for protein identification.[1] Sequence coverage and protein identification score were improved by combining mass data obtained before and after dansylation. The ionization efficiency of arginine-containing peptides is higher than that of lysine-containing peptides.[2] Based on these results, guanidination[3–7] or amidination[8,9] of the ε-amino group of lysine residues was used for signal enhancement of lysine-containing peptides and for peptide quantification.[7,8] Wa *et al.* examined experimental factors such as the type of matrix and the protein digestion method to obtain high sequence coverage in MALDI-TOF MS using human serum albumin as the model protein.[10]

Recently, MS-based quantification was performed by stable-isotope labeling of proteins or tryptic peptides.[11] Many methods have been developed for the incorporation of stable isotopes. Metabolic labeling using labeled nutrients,[12] chemical labeling of proteins[13] or peptides,[14–19] using isotope-coded reagent, and enzymatic labeling[20] are widely used. In the chemical labeling method, isotope-coded reagents target reactive sites on a protein or peptide, such as the sulfhydryl group of cysteine,[14,15] N-terminal amine,[16,17] ε-amino group of lysine,[7,8] tryptophan,[18] and the C-terminal carboxyl group.[19] The isotope-coded affinity tag (ICAT) method reported in 1999 by Gygi *et al.*[14] is the most widely used. In that method, the sulfhydryl group of cysteine is selectively modified with a biotin-conjugated reagent prior to protease treatment. As only cysteine-containing peptides are labeled and isolated, peptide mixtures are less complex. However, for proteins having no cysteine residues, the ICAT method is not applicable. Further, the large size of the ICAT reagent increases the complexity of tandem mass spectral (MS/MS) measurements because it is fragmented as well. Chemical modification methods targeting amino groups

**Correspondence to*: K. Kohda, Research Institute of Pharmaceutical Sciences, Musashino University, Shinmachi Nishitokyo-shi, Tokyo 202-8585, Japan.
E-mail: kohda@musashino-u.ac.jp
Contract/grant sponsor: MEXT. HAITEKU.

have been extensively developed for the identification and quantification of proteins. In their study published in 2000, Münchbach *et al.* protected the ε-amino group of lysines by succinylation and labeled N-terminal amines of tryptic peptides with 1-(d_0/d_4-nicotinoyloxy)succinimide (d_0/d_4-Nic-NHS).[16] In 2003, we reported the syntheses of 1-(6-methylnicotinoyloxy)succinimide (6-CH_3-Nic-NHS), 1-(2,6-dimethylnicotinoyloxy)succinimide (2,6-diCH_3-Nic-NHS), and their d-labeled analogues (6-CD_3-Nic-NHS and 2,6-diCD_3-Nic-NHS), and showed that these reagents can be prepared easily and at a low cost.[21] In 2005, Schmidt *et al.* reported the isotope-coded protein label (ICPL) strategy in which d_0- or d_4-Nic-NHS was used to label proteins.[13] A method that has recently gained popularity is the isobaric 'tag for relative and absolute quantification' (iTRAQ) reported in 2004 by Ross *et al.*[17] In this approach, four reagents are used and the labeled peptides have the same mass value in MS, but the fragment ions derived from the reagents facilitate quantification in MS/MS. Moreover, this multiplex strategy allows measurement of four samples in a single analysis. The conversion of the ε-amino group of lysine into homoarginine (guanidination) has also two advantages for PMF-based methods.[3–7] First, it increases the sensitivity of lysine-containing peptides and, second, the C-terminal amino acids of tryptic peptides are identified.

N-Hydroxysuccinimidyl (NHS) esters are the most commonly used reagents for chemical modification of the amino groups of peptides[16,17] and proteins.[13] For the efficient modification of N-terminal amino groups, the derivatization is performed at high pH. However, at high pH, selectivity is lost and partial derivatization of the ε-amino groups of lysine residues and the hydroxyl groups of tyrosine residues also takes place. For the relative quantification of peptides and proteins by the chemical modification method using isotope-coded reagents, the native peptides should be derivatized by the reagents selectively and efficiently. However, it is difficult to derivatize only the N-terminal amino groups of peptides by pH control. Münchbach *et al.* protected the ε-amino groups of lysine residues by succinylation and selectively derivatized the N-terminal amino groups by 1-(d_0/d_4-nicotinoyloxy)succinimide (d_0/d_4-Nic-NHS) after digestion with Glu(Asp)C-protease (V8).[16]

Compounds **1** and **2** shown in Fig. 1 are amine-reactive reagents that we previously reported.[21] The reactivities of these two reagents for the amino group and the ionization potentials of peptides derivatized with these reagents are considered to be the same, because only the hydrogen in the methyl group is replaced with the isotope atom, deuterium. The molecular weight of reagent **2** differs from that of reagent **1** by 3 Da. This mass difference is useful for the analysis of peptide sequences (number of amino group) and the relative quantification of proteins by MS.

Our approach involves the complete derivatization of both the N-terminal amino group and the ε-amino group of lysine residues of tryptic peptides with the reagents, as shown in Fig. 1. In this study, first, the conditions for derivatization were optimized and the effect of the derivatization on the MALDI-TOF MS signal intensity was studied using model peptides and tryptic peptides of model proteins. Next, tryptic peptides of both a single protein and five-protein mixture were used to demonstrate the applicability of our method to protein identification. The dynamic range of the relative quantification was determined using a binary mixture containing **1** (d_0)- and **2** (d_3)-derivatized peptides of tryptic myoglobin. Finally, our method was applied to the relative quantification of a mixture of five proteins.

EXPERIMENTAL

Chemicals

Bovine serum albumin (BSA), myoglobin from horse heart, cytochrome c from horse heart, α-lactalbumin from bovine milk, lysozyme from chicken egg white, iodoacetamide (IAA), α-cyano-4-hydroxycinnamic acid (CHCA), ammonium bicarbonate, and trypsin (proteomics grade) were purchased from Sigma (St. Louis, MO, USA). DL-Dithiothreitol (DTT) and triethylammonium bicarbonate buffer (TEAB) were purchased from Fluka (St. Louis, MO, USA). HPLC grade acetonitrile, 10% ammonium hydroxide (NH_4OH), and trifluoroacetic acid (TFA) were purchased

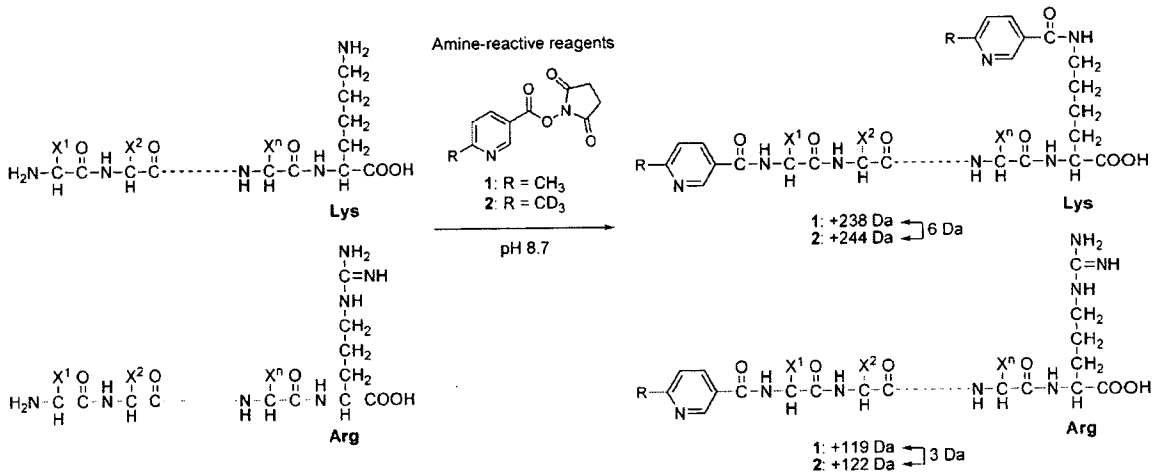

Figure 1. Chemical structures of amine-reactive reagents and scheme for derivatization. Peptides containing C-terminal lysine and arginine are derivatized with two and one molecules of reagent, respectively.

from Wako Pure Chemical Industries, Ltd. (Osaka, Japan). Bradykinin (RPPGFSPFR, $[M+H]^+ = 1060.57$) was purchased from Peptide Institute, Inc. (Osaka, Japan). Synthetic peptides RPPGFpSPFR ($[M+H]^+ = 1140.54$), TNASYSPRAK ($[M+H]^+ = 1094.56$), and TNApSYSPRAK ($[M+H]^+ = 1174.53$) were custom made by Sigma-Aldrich Japan (Tokyo, Japan). Amine-reactive reagents **1** and **2** shown in Fig. 1 were prepared by us as reported previously.[21]

Derivatization of model peptides

Method 1

A labeling reagent was dissolved in acetonitrile at a concentration of 50 mM. A model peptide was dissolved in water at a concentration of 1 mM. The model peptide solution (2 μL) was mixed with 50 mM NH_4HCO_3 (pH 7.8, 2 μL) or 50 mM TEAB (pH 8.7, 2 μL). To this peptide solution was added 20 μL of the reagent solution. The reaction mixture was mixed with a vortex mixer for 10 s and left at room temperature for 0.5–2 h. Then, it was quenched by adding 176 μL of 0.1% TFA (10 pmol/μL).

Method 2

A labeling reagent was dissolved in acetonitrile at a concentration of 100 mM. A model peptide was dissolved in water at a concentration of 5-200 pmol/μL. The model peptide solution (10 μL) was mixed with 100 mM TEAB (pH 8.7, 10 μL). To this peptide solution was added the reagent solution (20 μL), and the reaction mixture was stirred at room temperature for 1 h. Then, 20 μL of 10% NH_4OH was added and the mixture was stirred at room temperature for 2 h. The reaction was quenched by adding 10% TFA (100 μL) and the mixture was diluted with water (40 μL) to give a peptide solution of 0.25–10 pmol/μL.

Tryptic digestion of proteins

Stock solutions of proteins were prepared in 50 mM NH_4HCO_3 at a concentration of 1.5 μg/μL. Trypsin was dissolved in 1 mM HCl at a concentration of 1 μg/μL. Prior to tryptic digestion, the disulfide bonds of proteins were reduced with DTT and subsequently alkylated with IAA, as follows. A protein solution (100 μL) was added to a mixture of 50 mM NH_4HCO_3 (150 μL) and 200 mM DTT (20 μL) and the mixture was incubated at 95°C for 10 min. To the reduced sample was added 200 mM aqueous IAA (30 μL), and the mixture was stored in the dark at room temperature for 30 min. Trypsin digestion was performed by adding 3 μL of trypsin solution to 300 μL of reduced/carbamidomethylated solutions (1:50 w/w). The mixture was incubated at 37°C for 14 h. The digested sample (0.5 μg/μL) was stored at −30°C.

Derivatization of tryptic peptides

The labeling reagent was dissolved in acetonitrile at a concentration of 100 mM. Then 10 μL of the digested sample (0.5 μg/μL) was mixed with 10 μL of 100 mM TEAB (pH 8.7). To this solution was added 20 μL of the reagent solution and the mixture was stirred at room temperature for 1 h. Then, 20 μL of 10% NH_4OH was added and the mixture was stirred at room temperature for 2 h. The reaction was quenched by adding 80 μL of 10% TFA and the mixture was diluted with 60 μL of water.

MALDI-TOF MS analysis

MALDI-TOF mass spectra were acquired on an AXIMA-CFR instrument (Shimadzu/ Kratos, Kyoto, Japan). The operating conditions were as follows: nitrogen laser (337 nm); reflectron mode; detection of positive ions; acceleration voltage, 20 kV. Each spectrum was obtained by accumulating 50 shots. High-purity CHCA (proteomics grade) was used as the MALDI matrix throughout this study without further purification. CHCA was dissolved in 50% acetonitrile in 0.05% TFA at a concentration of 10 mg/mL. Samples for MS analysis were prepared by mixing 0.5 μL of the reaction mixture with 0.5 μL of the matrix solution on the MALDI target plate. The applied samples were allowed to dry at room temperature before transferring into the mass spectrometer.

Database search

The PMF search was carried out using MASCOT with the NCBInr database. The search parameters were as follows: Taxonomy, metazoan (animals); enzyme, trypsin; fixed modifications, carbamidomethyl (C), 6-CH_3-Nic (N-term and K); variable modifications, none; peptide tolerance, ±0.2 Da; mass values, $[M+H]^+$ and monoisotopic; and missed cleavages, 1.

RESULTS AND DISCUSSION

Derivatization of model peptides

To optimize the derivatization conditions, bradykinin (RPPGFSPFR, $[M+H]^+ = 1060.57$) and three synthetic peptides, RPPGFpSPFR ($[M+H]^+ = 1140.54$), TNASYSPRAK ($[M+H]^+ = 1094.56$), and TNApSYSPRAK ($[M+H]^+ = 1174.53$), were used as model peptides. The reasons why these peptides were used are that the C-terminal amino acid of the tryptic digest is arginine or lysine, and the phosphorylated peptide generally has low ionization efficiency in the positive ion mode due to the negatively charged phosphate group. The derivatization with reagent **1** was performed using 50 mM NH_4HCO_3 (pH 7.8) and 50 mM TEAB (pH 8.7) at room temperature for 0.5–2 h (method 1), and the MALDI mass spectra of the derivatized peptides are shown in Fig. 2. Figures 2(a)–2(c) show the MALDI mass spectra of RPPGFSPFR, RPPGFpSPFR, and TNASYSPRAK derivatized with reagent **1** at pH 7.8 for the indicated times, respectively. Under these conditions, no signals of the native peptide were observed in all cases. In the MALDI mass spectra of peptides containing C-terminal arginine, only the signal of a mono-derivatized peptide was observed at m/z 1179.68 (*) and 1259.61 (*), as shown in Figs. 2(a) and 2(b), respectively. In contrast, in the MALDI mass spectrum of the peptide containing C-terminal lysine, two signals corresponding to mono-derivatized and di-derivatized peptides were observed at m/z 1213.43 (*) and 1332.46 (**), as shown in Fig. 2(c). This is because two amino groups exist at both the N-terminal amino acid and the ε-position of lysine. On the other hand, Figs. 2(d)–2(f) show the MALDI mass spectra after derivatization at pH 8.7. Under this high pH condition,

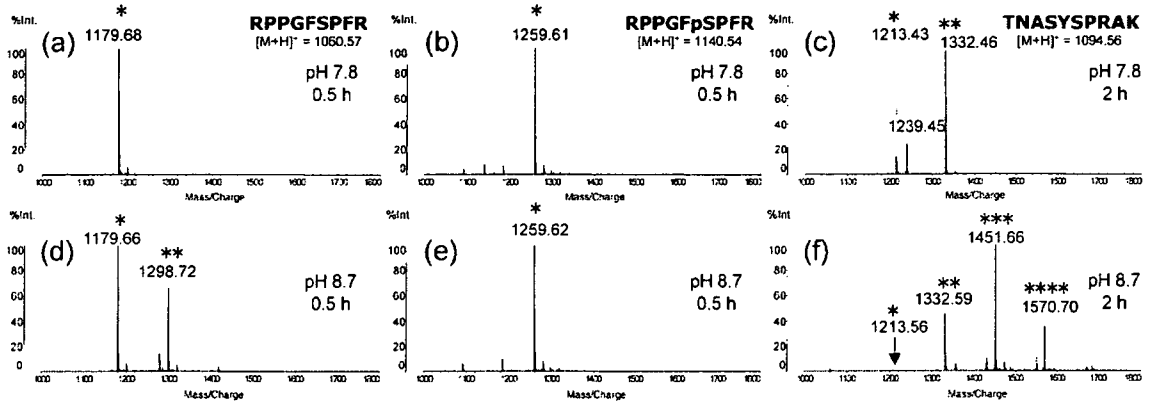

Figure 2. Comparison of reactivity of reagent **1** toward amino groups of peptides at pH 7.8 and pH 8.7. MALDI mass spectra of model peptides derivatized with reagent **1** are shown: (a) RPPGFSPFR, pH 7.8, 0.5 h; (b) RPPGFpSPFR, pH 7.8, 0.5 h; (c) TNASYSPRAK, pH 7.8, 2 h; (d) RPPGFSPFR, pH 8.7, 0.5 h; (e) RPPGFpSPFR, pH 8.7, 0.5 h; and (f) TNASYSPRAK, pH 8.7, 2 h. Number of asterisks (*) indicates the number of labels introduced into the peptide by the derivatization. A volume of 5 pmol of peptide was spotted on MALDI sample plate.

the derivatization of the hydroxyl groups also proceeded. Thus, in the MALDI mass spectrum of serine-containing RPPGFSPFR (Fig. 2(d)), the signal of the di-derivatized peptide that was not observed at pH 7.8 was observed at m/z 1298.72 (**). In the MALDI mass spectrum of RPPGFpSPFR shown in Fig. 2(e), the signal of the di-derivatized peptide was not observed because the hydroxyl group of the serine residue was blocked by the phosphorylation. From these results, it was concluded that, at pH 8.7, the hydroxyl group of the serine residue was also derivatized while the arginine residue was not. In TNASYSPRAK, two amino groups were completely derivatized at pH 8.7, as shown in Fig. 2(f), and its MALDI mass spectrum showed no signal of a mono-derivatized peptide at m/z 1213.56 (*). On the other hand, two signals corresponding to tri-derivatized and tetra-derivatized peptides were further observed at m/z 1451.66 (***) and 1570.70 (****). These two signals may be due to derivatization of the hydroxyl groups of the two serine residues rather than derivatization of the N-terminal amino group and the ε-amino group of lysine residue. To use the amine-reactive reagents for quantitative analysis, the reagents should be incorporated only into the N-terminal amino group of a peptide or both the N-terminal amino group and the ε-amino group of the lysine residue. However, as described above, it is difficult to derivatize only the N-terminal amino group by pH control. From these results, we devised the following approach. First, both the N-terminal amino group and the ε-amino group of lysine residue were completely derivatized at pH 8.7 although some esterification of hydroxyl groups of tyrosine, serine, and threonine proceeded. Second, the esterification site was cleaved off by hydrolysis with ammonium hydroxide. Figure 3 shows the MALDI mass spectra of the model peptides before (Figs. 3(a) and 3(b)) and after (Figs. 3(c) and 3(d)) derivatization with reagent **1** using method 2. Figure 3(c) shows the MALDI mass spectrum of bradykinin (RPPGFSPFR, $[M+H]^+ = 1060.57$)

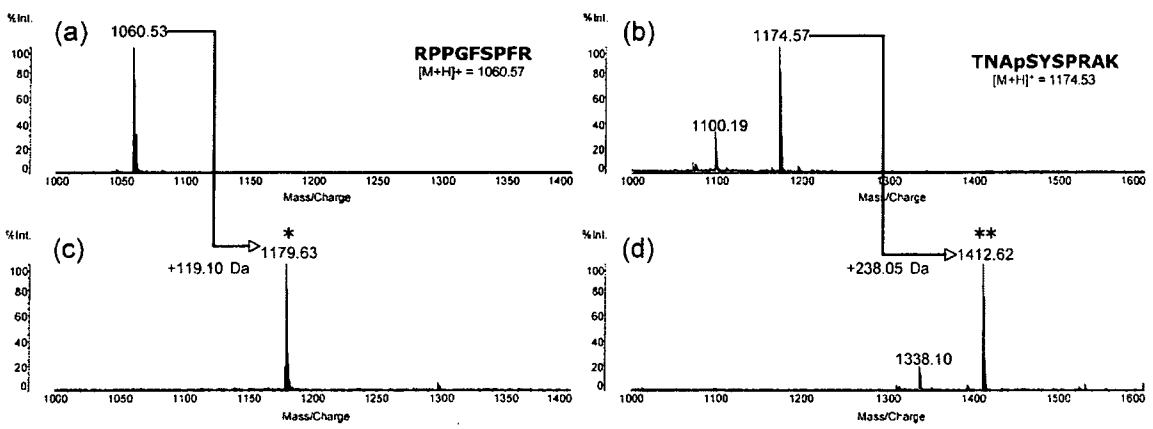

Figure 3. MALDI spectra of model peptides before and after derivatization. (a, b) MALDI spectra of 125 fmol of bradykinin (RPPGFSPFR) and 1.25 pmol of synthetic phosphorylated peptide (TNApSYSPRAK), respectively. (c, d) MALDI spectra of 125 fmol of bradykinin and 1.25 pmol of the phosphorylated peptide after derivatization with reagent 1. Number of asterisks (*) indicates the number of labels introduced into the peptide by the derivatization. Signals at *m/z* 1100.19 in (b) and *m/z* 1338.10 in (d) are due to impurities in the sample.

after derivatization. The mass increase (+119 Da) of the derivatized bradykinin (m/z 1179.63) corresponded to a mono-adduct at the N-terminal amino group. On the other hand, Fig. 3(d) shows the MALDI mass spectrum of the synthetic phosphorylated peptide (TNApSYSPRAK, $[M+H]^+ = 1174.53$) after derivatization. The mass increase (+238 Da) of the derivatized phosphorylated peptide (m/z 1412.62) corresponded to di-adducts. It is clear that the derivatization was completed at both the N-terminal amino group and the ε-amino group of the C-terminal lysine residue, because no signals of native, partially derivatized or multiply derivatized peptides were observed.

Derivatization of tryptic peptides of model proteins

We used myoglobin[5,16] as the model protein to demonstrate the applicability of our amine-derivatization method. Because myoglobin contains 19 lysines and 2 arginines, tryptic digestion of it generates many lysine-containing peptides.

The results of tryptic digestion of myoglobin are shown in Fig. 4 and Table 1. Figure 4(a) shows the MALDI mass spectrum of the digest without derivatization and Figs. 4(c) and 4(e) show those of the tryptic peptides derivatized with reagents **1** (d_0) and **2** (d_3), respectively. Figures 4(b), 4(d) and 4(f) show the MALDI mass spectra of Figs. 4(a), 4(c) and 4(e) in the low-mass range (m/z 400–700), respectively. Figure 4(g) shows the difference in sequence coverage of myoglobin with (underlined) and without (**bold**) derivatization. The peptide sequences of the detected peaks were assigned by MASCOT search and are summarized in Table 1 (matched mass values are shown in **bold**). Each peak in Fig. 4 was marked with an entry number shown in Table 1.

Before derivatization, the number of matched peptides was eight (**9**, **11–17**) and sequence coverage was 62% by MASCOT search, as shown in Fig. 4(g) in bold. On the other hand, as shown in Fig. 4(c), peptides **9**, **11–14**, **16**, and **17** were completely derivatized with reagent **1** and neither partially nor multiply derivatized signals were observed. The labeling efficiency of our reagents was almost the same as that of others reported.[16] Under these reaction conditions, no signals of derivatized peptide **15** were observed. It was evident that the signal intensities of peptides **9**, **11**, **13**, and **16** were improved by the derivatization (**9***, **11****, **13****, and **16*****) when compared with their signal intensities using that of peptide **14*** as standard. The number of asterisks (*) indicates the number of labels introduced into the peptide by the derivatization. Three peptides (**7****, **8*****, and **10*****) could be observed and matched by MASCOT search only after derivatization. After derivatization, the number of matched peptides was ten (**7–14**, **16**, and **17**) and sequence coverage was slightly increased to 64%, as shown in Fig. 4(g) with underlining. The minimal increase of the sequence coverage may be due to loss of high-mass peptide **15**. However, by using both native and derivatized peptides for database search, the sequence coverage was increased from 62% to

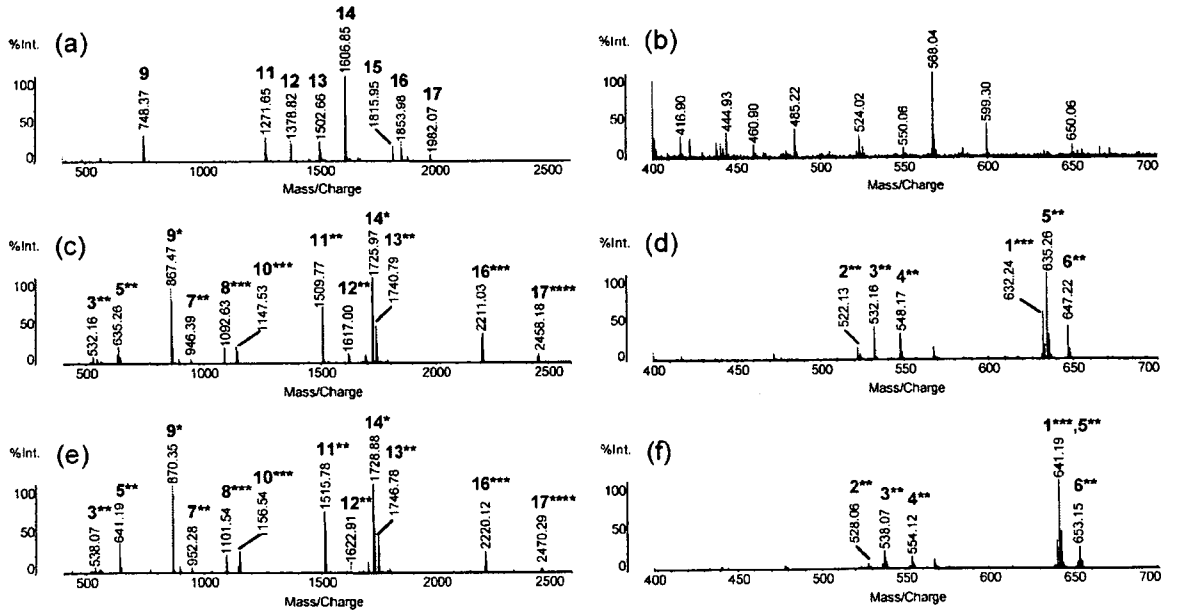

(g)
1 **GLSDGEWQQV LNVWGKVEAD IAGHGQEVLI RLFTGHPETL EK***FDKFKHLK*
51 TEAEMKASED LKKHGTVVLT ALGGILK*KKG* HHEAELKPLA QSHATK*HKIP*
101 IKYLEFISDA IIHVLHSKHP GDFGADAQGA MTKALELFRN DIAAK*YKELG*
151 FQG

Figure 4. MALDI mass spectra of tryptic myoglobin: (a, b) without derivatization; (c, d) with derivatization by reagent **1** (d_0); and (e, f) with derivatization by reagent **2** (d_3). (b), (d), and (f) are enlarged spectra of (a), (c), and (e), respectively. Peaks are marked with entry numbers shown in Table 1. Number of asterisks (*) indicates the number of labels introduced into the peptide by the derivatization. Each MALDI spot contained 12.5 ng (0.7 pmol) of myoglobin. (g) Sequence coverage in myoglobin before (**bold**) and after (underlined) derivatization.

Table 1. Sequences and mass values of myoglobin tryptic peptides

No.	Start–End	Native: Observed $[M+H]^+$	Native: Mr(calc) M	Sequence	d_0-Labeled: Mr(calc) M	d_0-Labeled: Observed $[M+H]^+$	d_3-Labeled: Observed $[M+H]^+$	Delta
1	78–79		274.20	K*K*	631.32	632.24	641.19	9
2	97–98		283.16	HK*	521.24	522.13	528.06	6
3	46–47		293.17	FK*	531.25	532.16	538.07	6
4	146–147		309.17	YK*	547.25	548.17	554.12	6
5	48–50		396.25	HLK*	634.33	635.26	641.19	6
6	43–45		408.20	FDK*	646.28	647.22	653.15	6
7	51–56		707.32	TEAEMK*	945.40	**946.39**	952.28	6
8	97–102		734.48	HK*IPIK*	1091.60	**1092.63**	1101.54	9
9	134–139	**748.37**	747.43	ALELFR	866.47	**867.47**	870.35	3
10	57–63		789.42	ASEDLK*K*	1146.54	**1147.53**	1156.54	9
11	32–42	**1271.65**	1270.66	LFTGHPETLEK*	1508.74	**1509.77**	1515.78	6
12	64–77	**1378.82**	1377.83	HGTVVLTALGGILK*	1615.91	**1617.00**	1622.91	6
13	119–133	**1502.66**	1501.66	HPGDFGADAQGAMTK*	1739.74	**1740.79**	1746.78	6
14	17–31	**1606.85**	1605.85	VEADIAGHGQEVLIR	1724.89	**1725.97**	1728.88	3
15	1–16	**1815.95**	1814.90	GLSDGEWQQVLNVWGK*	2052.98	N.D.	N.D.	—
16	80–96	**1853.98**	1852.95	GHHEAELK*PLAQSHATK*	2210.07	**2211.03**	2220.12	9
17	79–96	**1982.07**	1981.05	K*GHHEAELK*PLAQSHATK*	2457.21	**2458.18**	2470.29	12

N.D.: not detected.

74%. This increase of 12% is due to newly matched peptides **7****, **8*****, and **10***** after derivatization, as shown in Fig. 4(g) with only underlining and no bold. From these results, it was expected that sequence coverage could be increased by a combination of mass values obtained before and after derivatization.

By derivatization of one amino group with reagents **1** and **2**, the molecular weight of the derivatized peptide was increased by 119 and 122 Da, respectively, and the mass shift of the peptide derivatized with reagent **2** from that with reagent **1** was 3 Da. As shown in Fig. 4(c), signals of peptides **14**, **13**, **16**, and **17** were observed at m/z 1725.97 (**14***), 1740.79 (**13****), 2211.03 (**16*****), and 2458.18 (**17******) after derivatization with reagent **1** (d_0). These peptides contained one, two, three, and four amino groups, respectively, based on the mass increase and the sequence assignment by MASCOT search. As shown in Fig. 4(e), when reagent **2** (d_3) was used, the mass values shifted by 3 Da (**14***: m/z 1728.88), 6 Da (**13****: m/z 1746.78), 9 Da (**16*****: m/z 2220.12), and 12 Da (**17******: m/z 2470.29), respectively, from the corresponding peaks shown in Fig. 4(c). These results demonstrate that the mass shift by a combination of two reagents shows the number of labels introduced into the peptide (the number of amino groups). This method is useful for the identification of the C-terminal amino acid of the tryptic digest.

Figures 4(b), 4(d) and 4(f) are enlarged spectra (m/z 400–700) of Figs. 4(a), 4(c), and 4(e), respectively. Generally, it is difficult to use MALDI-TOF MS for the analysis of small molecules ($m/z < 500$ Da) because of the presence of a variety of matrix-related ions in the low-mass range below 500 Da. However, six signals were observed after derivatization with reagent 1 (Fig. 4(d)), which corresponded to di- and tripeptides **1–6** derivatized with reagent **1**, based on the mass increase. Comparing the spectrum of peptides derivatized with reagent 1 (d_0) (Fig. 4(d)) with that of ones derivatized with **2** (d_3) (Fig. 4(f)), the signals were found to be

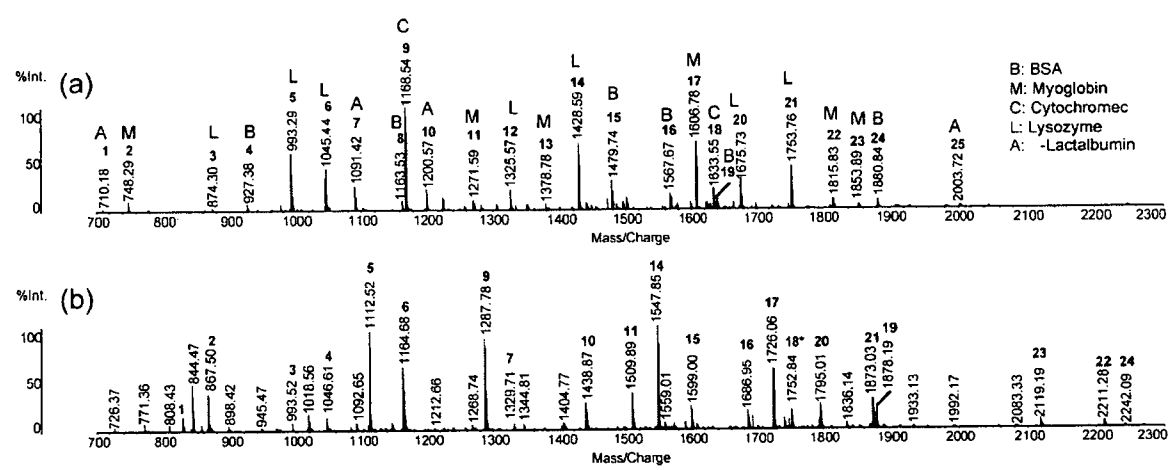

Figure 5. Derivatization of tryptic digest of five-protein mixture. (a) MALDI mass spectra of tryptic digests of a five-protein mixture. (b) MALDI mass spectrum of a mixture of tryptic digests derivatized with reagent **1**. Peaks are marked with entry numbers from Table 2.

Table 2. Sequences and mass values of tryptic peptides of the five-protein mixture

	Native						Labeled	
No.	Observed $[M+H]^+$	Mr (Calc) M	Protein	Start–End	Sequence	Number of labels	Mr (Calc) M	Observed $[M+H]^+$
1	710.18	709.32	α-Lac	25–29	CEVFR	1	828.36	829.39
2	748.29	747.43	Myo	134–139	ALELFR	1	866.47	867.50
3	874.30	873.41	Lys	33–39	HGLDNYR	1	992.45	993.52
4	927.38	926.49	BSA	161–167	YLYEIAR	1	1045.53	1046.61
5	993.29	992.39	Lys	80–86	WWCNDGR	1	1111.43	1112.52
6	1045.44	1044.54	Lys	135–143	GTDVQAWIR	1	1163.58	1164.68
7	1091.42	1090.51	α-Lac	134–141	LDQWLCEK	2	1328.59	1329.71
8	1163.53	1162.62	BSA	66–75	LVNELTEFAK	2	1400.70	N.D.
9	1168.54	1167.61	Cyt	28–38	TGPNLHGLFGR	1	1286.65	1287.78
10	1200.57	1199.65	α-Lac	118–127	VGINYWLAHK	2	1437.73	1438.87
11	1271.59	1270.66	Myo	32–42	LFTGHPETLEK	2	1508.74	1509.89
12	1325.57	1324.62	Lys	40–51	GYSLGNWVCAAK	2	1562.70	N.D.
13	1378.78	1377.83	Myo	64–77	HGTVVLTALGGILK	2	1615.91	N.D.
14	1428.59	1427.64	Lys	52–63	FESNFNTQATNR	1	1546.68	1547.85
15	1479.74	1478.79	BSA	421–433	LGEYGFQNALIVR	1	1597.83	1599.00
16	1567.67	1566.74	BSA	347–359	DAFLGSFLYEYSR	1	1685.78	1686.95
17	1606.78	1605.85	Myo	17–31	VEADIAGHGQEVLIR	1	1724.89	1726.06
18	1633.55	1632.76	Cyt	9–22	IFVQKCAQCHTVEK	3	1989.88	N.D.
19	1639.87	1638.93	BSA	437–451	KVPQVSTPTLVEVSR	2	1877.01	1878.19
20	1675.73	1674.79	Lys	116–130	IVSDGNGMNAWVAWR	1	1793.83	1795.01
21	1753.76	1752.83	Lys	64–79	NTDGSTDYGILQINSR	1	1871.87	1873.03
22	1815.83	1814.90	Myo	1–16	GLSDGEWQQVLNVWGK	2	2052.98	N.D.
23	1853.89	1852.95	Myo	80–96	GHHEAELKPLAQSHATK	3	2210.07	2211.28
24	1880.84	1879.91	BSA	508–523	RPCFSALTPDETYVPK	2	2117.99	2119.19
25	2003.72	2002.81	α-Lac	82–98	DDQNPHSSNICNISCDK	2	2240.89	2242.09

N.D.: not detected.

shifted by 6 or 9 Da according to the theoretical number of amino groups calculated from the sequence shown in Table 1. From these mass shifts and calculated mass values after derivatization, the sequence of the newly observed signals is matched with the calculated sequence, as shown in Table 1. Thus, owing to the increase in molecular weight and the improved ionization efficiency, this derivatization method was useful for the identification of small peptides such as di- and tripeptides. By using these small peptides **1–6** shown in Fig. 4(g) (*italics*), the sequence coverage was increased from 62% (without derivatization) to 82%.

From the above experiments, the following results were obtained. By using this derivatization method, both the N-terminal amino group and the ε-amino group of lysine were completely derivatized. In the case of a C-terminal arginine residue, only a mono-labeled peak (*) was observed. In contrast, in the case of C-terminal lysine residues, only a di- labeled peak (**) was observed. Owing to the increase in molecular weight, the ionization efficiency of small peptides ($m/z < 500$ Da) was significantly improved after derivatization.

To demonstrate the labeling efficiency of amine-reactive reagents for more complexity, a mixture of five proteins (BSA, myoglobin, cytochrome c, α-lactalbumin, and lysozyme) was used. The five-protein mixture was reduced with DTT, alkylated with IAA, and digested with trypsin. Tryptic peptides with or without derivatization were subjected to MALDI mass analysis. The MALDI mass spectra are shown in Fig. 5 and the sequences and mass values of the peptides are summarized in Table 2. Results showed that the labeling efficiency was almost quantitative to the tryptic peptides of protein mixture.

Effect of derivatization on MALDI signal intensities

To examine the effect of the derivatization on MALDI signal intensity, equal amounts of native and peptides derivatized with reagent **1** were mixed and the mixture was subjected to MALDI analysis. Figure 6 shows the MALDI mass spectra of

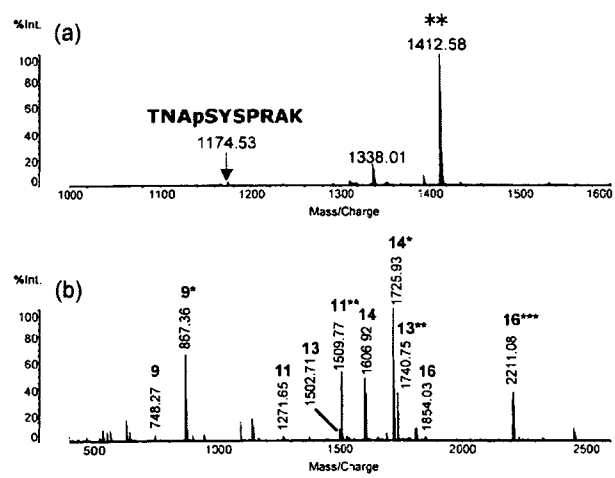

Figure 6. Effect of derivatization on MALDI signal intensity. (a) MALDI mass spectrum of a mixture containing equal amounts of native peptide TNApSYSPRAK and its peptide derivatized with reagent **1**. The signal at m/z 1338.01 is due to the impurity in the sample. (b) MALDI spectrum of a mixture containing equal amounts of native and derivatized tryptic myoglobin. Peaks are marked with entry numbers shown in Table 1. Number of asterisks (*) indicates the number of labels introduced into the peptide by the derivatization.

Table 3. Effect of derivatization on MALDI signal intensities

Entry	Start–End	Sequence	*m/z* Native	*m/z* Labeled	Signal enhancement (n = 12)
1	134–139	ALELFR (**9***/**9**)	748.27	867.36	11.7 ± 2.7
2	32–42	LFTGHPETLEK (**11****/**11**)	1271.65	1509.77	11.9 ± 2.9
3	119–133	HPGDFGADAQGAMTK (**13****/**13**)	1502.71	1740.75	5.0 ± 0.8
4	17–31	VEADIAGHGQEVLIR (**14***/**14**)	1606.92	1725.93	1.8 ± 0.4
5	80–96	GHHEAELKPLAQSHATK (**16*****/**16**)	1854.03	2211.08	8.1 ± 2.8

the mixture containing native and derivatized peptides. The signal-enhancing effect was calculated from the ratio of the signal intensities of the derivatized peptide to those of the native one (Table 3). In the case of the phosphorylated peptide, marked enhancement of ionization efficiency was observed by derivatization with reagent **1** (Fig. 6(a)). In the case of tryptic myoglobin, the derivatization increased detection sensitivity, as shown in Fig. 6(b), and the enhancement factor was approximately 2–11 (Table 3). The signal enhancement of the lysine-containing peptide was greater than that of the arginine-containing peptide. In the case of the arginine-containing peptide, the signal enhancement of the small peptide (**9***/**9**: 11.7) was greater than that of the large peptide (**14***/**14**: 1.8).

Relative quantification by MALDI-TOF MS

To examine the dynamic range of the quantitative analysis, tryptic peptides from myoglobin were used. Two samples (A and B) containing tryptic peptides at different concentrations were prepared (A: 0.1 μg/μL, and B: 0.5, 0.2, 0.1, and 0.05 μg/μL). Samples A and B were derivatized with isotope-coded light (d_0: **1**) and heavy reagents (d_3: **2**), respectively. Equal volumes of solutions derivatized with reagents **1** and **2** were mixed, and the mixture was desalted, concentrated, and subjected to MALDI analysis (2-derivatized, 90–900 fmol). The d_3/d_0 ratio for doublets spaced by 3 Da was calculated manually using intensities of monoisotopic peaks (*m/z* 1729/1726). Figures 7(a)–7(d) show the enlarged MALDI-TOF mass spectra of d_0- or d_3-derivatized tryptic peptides of myoglobin (VEADIAGHGQEVLIR). The calculated d_3/d_0 ratios were 5, 2, 1, and 0.5. The spectra showed that the signal intensities of the doublets spaced by 3 Da changed with the sample ratio. The experimental data are summarized in Figs. 7(e) and 7(f). The correlation coefficient and slope between the expected ratio and the observed ratio for the tryptic peptide VEADIAGHGQEVLIR (residues 17–31) were $R^2 = 0.9921$ and 1.08, respectively, as

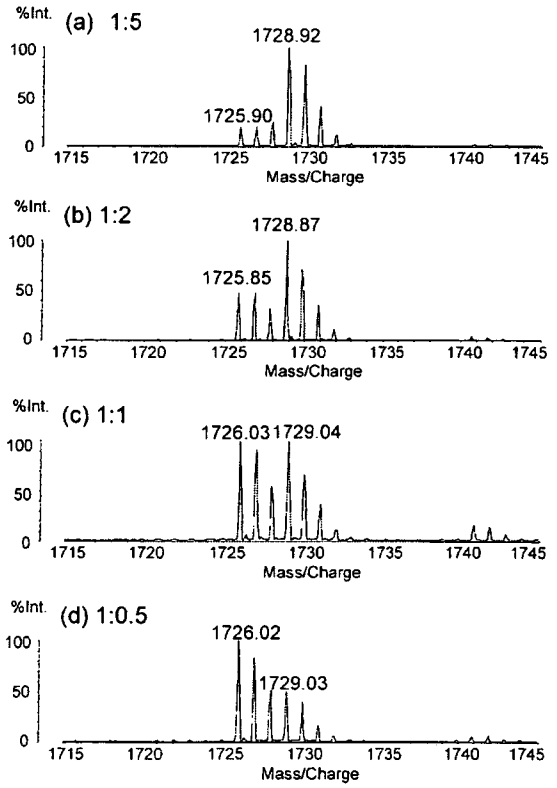

(e)

Expected ratio (d_3/d_0)	Observed ratio (d_3/d_0)	%Error
5.0	5.37 ± 0.68	7
2.0	1.76 ± 0.20	12
1.0	0.99 ± 0.12	1
0.5	0.58 ± 0.06	15

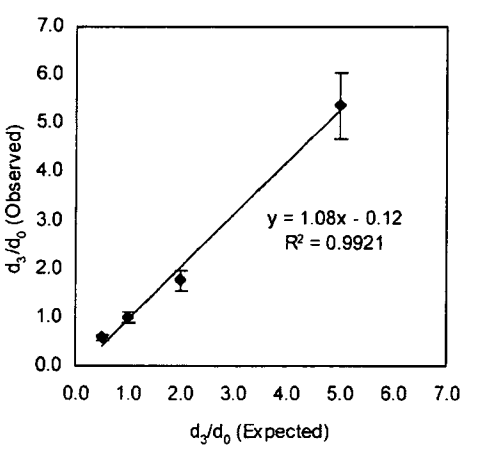

Figure 7. Relative quantification of tryptic digest of myoglobin. Enlarged MALDI mass spectra of peptide VEADIAGHGQEVLIR (residues 17–31) derivatized with d_0-reagent **1** (*m/z* 1726) and d_3-reagent **2** (*m/z* 1729). The ratios of the amounts of d_0-derivatized myoglobin and d_3-derivatized one were (a) 1:5, (b) 1:2, (c) 1:1, and (d) 1:0.5.

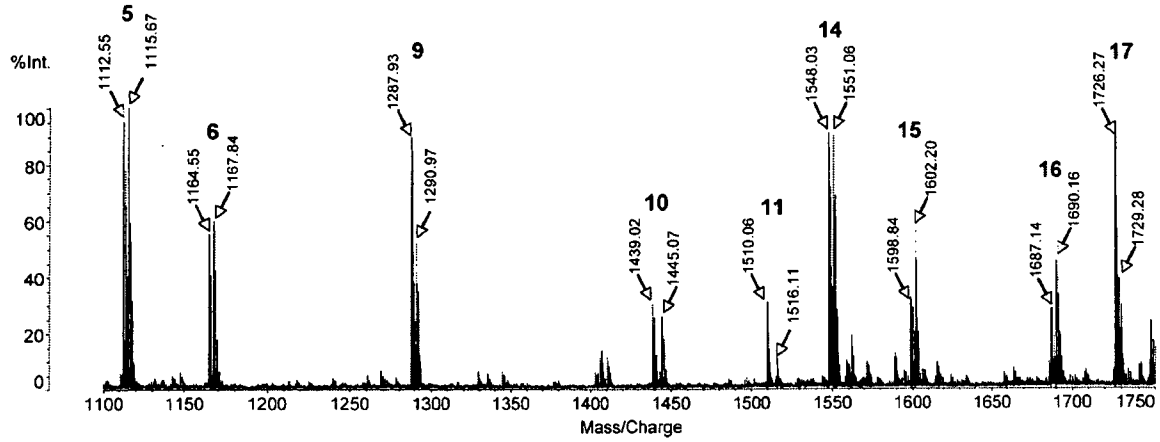

Figure 8. Relative quantification of five-protein mixture. MALDI mass spectrum of a mixture of tryptic digests derivatized with reagents **1** (d_0) and **2** (d_3) is shown. Peaks are marked with entry numbers from Table 2.

shown in Fig. 7(f). These results indicate the potential use of this derivatization method that employs isotope-coded **1** and **2** in the relative quantification of protein by MALDI-TOF MS analysis.

Relative quantification of the five-protein mixture

Two mixtures (A and B) containing the same five proteins at different concentrations were prepared and the applicability of our method was examined. Mixtures A and B consisted of BSA (A: 0.2 μg/μL, B: 0.4 μg/μL), myoglobin (A: 0.2 μg/μL, B: 0.1 μg/μL), cytochrome c (A: 0.2 μg/μL, B: 0.1 μg/μL), lysozome (A: 0.2 μg/μL, B: 0.2 μg/μL), and α-lactalbumin (A: 0.2 μg/μL, B: 0.2 μg/μL), respectively. Samples A and B were reduced, alkylated, digested, and derivatized with reagents **1** and **2** according to the procedure described above. Equal volumes of derivatized samples A and B were mixed and a portion of the mixture was subjected to MALDI analysis. The peptide ratio was calculated from the intensities of the monoisotopic peaks. The MALDI mass spectrum is shown in Fig. 8 and the sequences and ratios of the peptides are summarized in Table 4. Even in the mixtures of five proteins, the protein ratios (d_3/d_0) gave satisfactory values.

CONCLUSIONS

We have demonstrated the applicability of amine-reactive reagents **1** and **2** to the identification and quantification of proteins using the tryptic peptides of model proteins. Our approach involves complete derivatization of both the N-terminal amino groups and the ε-amino groups of lysine residues with these reagents. Labeling efficiency was almost quantitative to the tryptic peptides of both a single protein and five-protein mixture. Through the derivatization, the basic moiety of the reagent is incorporated into the amino group, improving the ionization efficiency of the peptide. Isotope-coded reagent **2** (d_3) is useful for the relative quantification of proteins by MS. Moreover, this approach has one advantage for peptide sequence analysis: The peptides generated by tryptic digestion of proteins contain C-terminal arginine or lysine, and these peptides are derivatized with one or two molecules of the reagent, respectively. Comparison of peptides derivatized with reagents **1** (d_0) and **2** (d_3) showed that the derivatization gave mass differences of 3 and 6 Da in arginine- and lysine-containing peptides, respectively. Taken together, the results show that our derivatization method is simple and useful for the identification and relative quantification of proteins.

Table 4. Sequence identification and quantification of proteins in the five-protein mixture

m/z						Ratio (d_3/d_0)				
d_0-Labeled	d_3-Labeled	No. (Table 2)	Protein	Start–End	Sequence	Expected	Obseved	Average	SD	%Error
1598.84	1602.20	**15**	BSA	421–433	LGEYGFQNALIVR	2.0	1.9	1.8	0.14	10
1687.14	1690.16	**16**	BSA	347–359	DAFLGSFLYEYSR	2.0	1.7			
1510.06	1516.11	**11**	Myo	32–42	LFTGHPETLEK	0.5	0.3	0.4	0.14	20
1726.27	1729.28	**17**	Myo	17–31	VEADIAGHGQEVLIR	0.5	0.5			
1287.93	1290.97	**9**	Cyt	28–38	TGPNLHGLFGR	0.5	0.5			0
1112.55	1115.67	**5**	Lys	80–86	WWCNDGR	1.0	1.1	1.1	0.06	10
1164.55	1167.84	**6**	Lys	135–143	GTDVQAWIR	1.0	1.1			
1548.03	1551.06	**14**	Lys	52–63	FESNFNTQATNR	1.0	1.0			
1439.02	1445.07	**10**	α-Lac	118–127	VGINYWLAHK	1.0	0.7			30

Acknowledgements

This work was partly supported by MEXT. HAITEKU (2006).

REFERENCES

1. Park SJ, Song JS, Kim HJ. *Rapid Commun. Mass Spectrom.* 2005; **19**: 3089.
2. Krause E, Wenschuh H, Jungblut PR. *Anal. Chem.* 1999; **71**: 4160.
3. Hale JE, Butler JP, Knierman MD, Becker GW. *Anal. Biochem.* 2000; **287**: 110.
4. Beardsley RL, Karty JA, Reilly JP. *Rapid Commun. Mass Spectrom.* 2000; **14**: 2147.
5. Beardsley RL, Reilly JP. *Anal. Chem.* 2002; **74**: 1884.
6. Cagney G, Emili A. *Nat. Biotechnol.* 2002; **20**: 163.
7. Brancia FL, Montgomery H, Tanaka K, Kumashiro S. *Anal. Chem.* 2004; **76**: 2748.
8. Beardsley RL, Reilly JP. *J. Proteome Res.* 2003; **2**: 15.
9. Beardsley RL, Sharon LA, Reilly JP. *Anal. Chem.* 2005; **77**: 6300.
10. Wa C, Cerny R, Hage DS. *Anal. Biochem.* 2006; **349**: 229.
11. Ong SE, Mann M. *Nat. Chem. Biol.* 2005; **1**: 252.
12. Ong SE, Blagoev B, Kratchmarova I, Kristensen DB, Steen H, Pandey A, Mann M. *Mol. Cell. Proteomics* 2002; **1**: 376.
13. Schmidt A, Kellermann J, Lottspeich F. *Proteomics* 2005; **5**: 4.
14. Gygi SP, Rist B, Gerber SA, Turecek F, Gelb MH, Aebersold R. *Nat. Biotechnol.* 1999; **17**: 994.
15. Kurono S, Kurono T, Komori N, Niwayama S, Matsumoto H. *Bioorg. Med. Chem.* 2006; **14**: 8197.
16. Münchbach M, Quadroni M, Miotto G, James P. *Anal. Chem.* 2000; **72**: 4047.
17. Ross PL, Huang YN, Marchese JN, Williamson B, Parker K, Hattan S, Khainovski N, Pillai S, Dey S, Daniels S, Purkayastha S, Juhasz P, Martin S, Bartlet-Jones M, He F, Jacobson A, Pappin DJ. *Mol. Cell. Proteomics* 2004; **3**: 1154.
18. Kuyama H, Watanabe M, Toda C, Ando E, Tanaka K, Nishimura O. *Rapid Commun. Mass Spectrom.* 2003; **17**: 1642.
19. Goodlett DR, Keller A, Watts JD, Newitt R, Yi EC, Purvine S, Eng JK, Haller PV, Aebersold R, Kolker E. *Rapid Commun. Mass Spectrom.* 2001; **15**: 1214.
20. Yao X, Freas A, Ramirez J, Demirev PA, Fenselau C. *Anal. Chem.* 2001; **73**: 2836.
21. Tsumoto H, Murata C, Miyata N, Taguchi R, Kohda K. *Chem. Pharm. Bull.* 2003; **51**: 1399.

Available online at www.sciencedirect.com
ScienceDirect
Analytica Chimica Acta 599 (2007) 315–319
ANALYTICA CHIMICA ACTA
www.elsevier.com/locate/aca

Iron-chelating agents never suppress Fenton reaction but participate in quenching spin-trapped radicals

Li Linxiang[a], Yoshihiro Abe[a,*], Kiyotada Kanagawa[a], Tomoko Shoji[a], Tadahiko Mashino[a], Masataka Mochizuki[a], Miho Tanaka[b], Naoki Miyata[c]

[a] *Kyoritsu University of Pharmacy, 1-5-30 Shibakoen, Minato, Tokyo 105-8512, Japan*
[b] *Tokyo University of Marine Science and Technology, Minato, Tokyo 108-8477, Japan*
[c] *Nagoya City University, Faculty of Pharmaceutical Sciences, 3-1 Tanabe-dori, Mizuho, Nagoya 467-8603, Japan*

Received 4 June 2007; received in revised form 1 August 2007; accepted 3 August 2007
Available online 6 August 2007

Abstract

Hydroxyl radical formation by Fenton reaction in the presence of an iron-chelating agent such as EDTA was traced by two different assay methods; an electron spin resonance (ESR) spin-trapping method with 5,5-dimethyl-1-pyrroline *N*-oxide (DMPO), and high Performance liquid chromatography (HPLC)-fluorescence detection with terephthalic acid (TPA), a fluorescent probe for hydroxyl radicals. From the ESR spin-trapping measurement, it was observed that EDTA seemed to suppress hydroxyl radical formation with the increase of its concentration. On the other hand, hydroxyl radical formation by Fenton reaction was not affected by EDTA monitored by HPLC assay. Similar inconsistent effects of other iron-chelating agents such as nitrylotriacetic acid (NTA), diethylenetriamine penta acetic acid (DTPA), oxalate and citrate were also observed. On the addition of EDTA solution to the reaction mixture 10 min after the Fenton reaction started, when hydroxyl radical formation should have almost ceased but the ESR signal of DMPO-OH radicals could be detected, it was observed that the DMPO-OH• signal disappeared rapidly. With the simultaneous addition of Fe(II) solution and EDTA after the Fenton reaction ceased, the DMPO-OH• signal disappeared more rapidly. The results indicated that these chelating agents should enhance the quenching of [DMPO-OH]• radicals by Fe(II), but they did not suppress Fenton reaction by forming chelates with iron ions.

Keywords: Electron spin resonance; 5,5-Dimethyl-1-pyrroline *N*-oxide; Hydroxyl radical; Fenton reaction; Ethylenediamine tetraacetic acid

1. Introduction

The spin-trapping method with 5,5-dimethyl-1-pyrroline *N*-oxide (DMPO) has been widely accepted as an assay technique to measure the hydroxyl radical scavenging activity of a compound, where the Fenton reaction has been widely used as the source of hydroxyl radicals. In the usual experimental procedure, a compound expected to scavenge hydroxyl radicals is added to the reaction mixture before starting the Fenton reaction. When the electron spin resonance (ESR) signal of the DMPO-OH adducts decreases or disappears, it can be concluded that hydroxyl radicals were scavenged by the additive, or that hydroxyl radical formation was suppressed by the additive only when supporting observations exist which could confirm the formation of a strong chelate with iron ions. Even though such chelate formation should be present, there is no evidence to confirm that hydroxyl radical formation must be suppressed by chelation. As we pointed out previously [1], the signal intensity of DMPO-OH radicals in ESR spectra should diminish in the following cases (Fig. 1):

(1) OH radical formation is suppressed by the additive,
(2) the formed OH radical is scavenged by the additive, or
(3) the formed DMPO-OH radical ([DMPO-OH]•) is quenched by the additive in a short period.

We also demonstrated that Fe(II) ions should quench [DMPO-OH]• radicals. In the same report, we showed that mannitol, which is considered to be a hydroxyl radical scavenger, did scavenge hydroxyl radicals but had little effect on the signal decay of [DMPO-OH]• in ESR, whereas phosphate buffer

* Corresponding author. Tel.: +81 3 5400 2673; fax: +81 3 5400 2643.
E-mail address: abe-ys@kyoritsu-ph.ac.jp (Y. Abe).